Scale free chaos in swarms

R. González-Albaladejo,[1,2] A. Carpio,[1,2] and L. L. Bonilla[2,3]
[1)]*Departamento de Matemática Aplicada, Universidad Complutense de Madrid, 28040 Madrid, Spain*
[2)]*Gregorio Millán Institute for Fluid Dynamics, Nanoscience and Industrial Mathematics, Universidad Carlos III de Madrid, 28911 Leganés, Spain*
[3)]*Department of Mathematics, Universidad Carlos III de Madrid, 28911 Leganés, Spain*

(*Electronic mail: bonilla@ing.uc3m.es)

(Dated: 18 August 2022)

Swarms are examples of collective behavior of insects, which are singular among manifestations of flocking. Swarms possess strong correlations but no global order and exhibit finite-size scaling with a dynamic critical exponent $z \approx 1$. We have discovered a phase transition of the three-dimensional harmonically confined Vicsek model that exists for appropriate noise and small confinement strength. On the critical line of confinement versus noise, swarms are in a state of scale-free chaos that can be characterized by minimal correlation time, correlation length proportional to swarm size and topological data analysis. The critical line separates dispersed single clusters from confined multicluster swarms. Susceptibility, correlation length, dynamic correlation function and largest Lyapunov exponent obey power laws. Their critical exponents agree with those observed in natural midge swarms, unlike values obtained from the order-disorder transition of the standard Vicsek model which confines particles by artificial periodic boundary conditions.

I. INTRODUCTION

For reasons that are not well understood, many biological systems live close to criticality, which induces power law behavior of macroscopic variables[1,2]. Examples include networks of neurons in vertebrate retinas[1], amino acid frequencies in proteins[3], or flocking phenomena in animals[4–6]. The components of many of these systems interact only with closer ones, defined either metrically or topologically[6]. However, the maximum correlation length separating two mutually influencing components is proportional to the system size. Macroscopic variables depend only on this correlation length which, in turn, scales with the distance to the critical surface. Power laws arise from this scale-free behavior, which can be exploited using ideas from equilibrium phase transitions[7]. Apropos, insect swarms provide particularly rich empirical data[6,8–10].

Male midges and other diptera form swarms near visual markers to attract females for reproductive purposes[8–10]. Natural swarms present collective behavior and strong correlations but not global order. The polarization order parameter (the mean of the directions of insect velocities) is quite small but the correlation length (measuring the largest distance between two insects whose velocity fluctuations still influence each other) is proportional to the swarm size[13]. It is also much larger than all other length scales, such as insect size, average separation between insects, etc. Macroscopic variables, such as the correlation length, the susceptibility to polarization changes and the dynamic correlation, follow power laws as functions of the distance to criticality, with critical exponents that differ from those of equilibrium and many nonequilibrium phase transitions[7,11–13]. Cavagna and coworkers have shown that the characteristic timescale, static and dynamic connected correlation functions depend on the control parameters (density, noise, ...) only through the correlation length. This is the finite-size scaling hypothesis, which is similar to that found in second-order equilibrium phase transitions[7,14]. Finite-size scaling allows us to extrapolate power laws of macroscopic variables obtained for finite N to the case of infinitely many particles, which characterize phase transitions[15]. For natural swarms, Cavagna *et al* use a nearest neighbor distance rescaled with insect size as control parameter because insect density or noise cannot be directly observed[11–13]. The measured critical exponents for the susceptibility and the characteristic timescale would identify the swarm universality class[11–13].

Midges communicate acoustically with neighbors within a few insect sizes. Swarm formation is triggered by a marker placed on the floor. While small swarms track the marker shape, larger swarms larger are more isotropic and shape independent[10]. Isotropic swarms lack translation invariance and their cohesion may be explained by a confining harmonic potential[16]. Thus, the harmonically confined three dimensional Vicsek model (VM) could provide a first description of swarms: N particles subject to discrete time dynamics under a harmonic potential align their velocities to the average velocity of all particles within their sphere of influence plus an alignment noise. The particles move with constant speed. Due to gravity, the vertical spring constant is smaller than the horizontal ones, and larger swarms are vertically elongated[16]. Here we consider a single spring constant for the sake of simplicity. The usual VM[17–20] confines particles in a box with periodic boundary conditions, is translationally invariant and exhibits a flocking order-disorder phase transition at a critical noise. This transition changes from continuous to discontinuous beyond a certain particle number[20]. Nevertheless, for smaller N, finite-size scaling holds as if the order-disorder transition were second order. The resulting power laws have critical exponents different from those measured in natural swarms[11–13]. From a modeling point of view, this should not be surprising. Periodic boundary conditions may apply to a swarm with many insects occupying a volume so large that boundaries do not influence its interior. Natural midge swarms comprise at most several hundred insects, form about a marker

and are not invariant under translations.

We have discovered a line of phase transitions deep inside the ordered phase of the harmonically confined VM which are characterized by scale-free chaos obeying finite-size scaling. Unlike the standard VM, for small confinement strength and alignment noise well below the order-disorder phase transition of the standard VM, the confined VM exhibits chaotic behavior. On the critical line in the confinement versus noise plane, the chaotic attractor is scale-free, all macroscopic variables obey power laws with the correlation length, which scales as the size of the swarm. The critical line is characterized by minimal correlation time and it separates single from multicluster chaotic swarms. In this paper, we describe the scale-free-chaos phase transition, calculate its critical exponents and find a power law for the *positive* LLE. Numerical evidence suggests that both the critical confinement and LLE vanish for infinitely many insects. Moreover, our numerically obtained critical exponents for the transition between single and multicluster chaotic attractors are compatible with observations of natural swarms.

The rest of the paper is as follows. We present the confined Vicsek model in Section II and find different attractors as the confinement parameter decreases from a large value. Among them, period 2, period 4 periodic solutions, quasiperiodic solutions, large period solutions, and chaotic attractors with positive Lyapunov exponents. Section III discusses algorithms to calculate the largest Lyapunov exponent (LLE) and how to distinguish deterministic and noisy chaos and noise, using Gao *et al*'s scale dependent Lyapunov exponents. Section IV uses ideas from statistical physics, modified correlation functions, and finite-size scaling to obtain the main results of the paper: the existence of a line of phase transitions within the noisy chaos region of the parameter space. Section V uses topological data analysis to characterize the phase transitions from single cluster to multicluster chaotic attractors. Section VI discusses our findings and it contains our conclusions whereas the Appendices are devoted to technical matters. Appendix A describes our nondimensionaization of the confined Vicsek model. Appendix B describes the Benettin algorithm, scale dependent Lyapunov exponents and the Gao-Zheng algorithm to extract the largest Lyapunov exponent from high dimensional reconstructions of the chaotic attractor using lagged coordinates. Appendix C discusses dynamic and static correlation functions, how to calculate them and different definitions of critical lines at finite number of particles.

II. CONFINED VICSEK MODEL

We have nondimensionalized the VM governing equations using data from natural swarms (see Appendix A):

$$\begin{aligned}\mathbf{x}_i(t+1) &= \mathbf{x}_i(t) + \mathbf{v}_i(t+1),\\ \mathbf{v}_i(t+1) &= v_0 \mathscr{R}_\eta \left[\Theta\left(\sum_{|\mathbf{x}_j - \mathbf{x}_i| < R_0} \mathbf{v}_j(t) - \beta \mathbf{x}_i(t) \right) \right], \quad (1)\end{aligned}$$

where $i = 1, \ldots, N$, $v_0 = 1$ is a constant speed, $R_0 = 1$, β is the confinement strength. The position and velocity of the ith particle at time t are $\mathbf{x}_i(t)$ and $\mathbf{v}_i(t)$, respectively. In (1), $\Theta(\mathbf{x}) = \mathbf{x}/|\mathbf{x}|$ and $\mathscr{R}_\eta(\mathbf{w})$ rotates the unit vector $\mathbf{w}$ randomly within a spherical cone centered at its origin and spanning a solid angle in $(-\frac{\eta}{2}, \frac{\eta}{2})$. The 2D VM is defined similarly. Initially, the particles are randomly placed within a sphere with unit radius and the particle velocities point outwards.

The VM exhibits a variety of attractors for different values of confinement β and alignment noise η, as depicted in Fig. 1. For large β and $\eta = 0$, the swarm occupies the unit sphere and it is pulsating with period 2: all particles reverse their velocities at each time step. The center of mass (CM) of the swarm occupies two positions ($\beta = 600$) or four ($\beta = 300$, period 4 attractor) as shown in Fig. 1(a). As β decreases, there appear quasiperiodic attractors interspersed with periodic attractors with higher periods, and chaotic attractors, cf. Fig. 1(b)-(f).

Fig. 2(a)-(b) show how different attractors in Fig. 1 appear as the parameter β changes. Periodic and quasiperiodic attractors exist for large confinement values and quasiperiodicity turns into chaos below $\beta \approx 30$. The chaotic attractor first looks like a torus and its central hole is filled as β decreases, cf. Figs. 1(d)-(f). As shown in cf. Fig. 2(c), tuning the alignment noise produces similar attractors, there are parameter regions where noise induces chaos and there are scale-free chaos transitions, which will be discussed later.

III. DETERMINISTIC AND NOISY CHAOS

For small confinement values and appropriate noise, the VM exhibits chaotic attractors characterized by positive values of the largest Lyapunov exponent (LLE). It is important

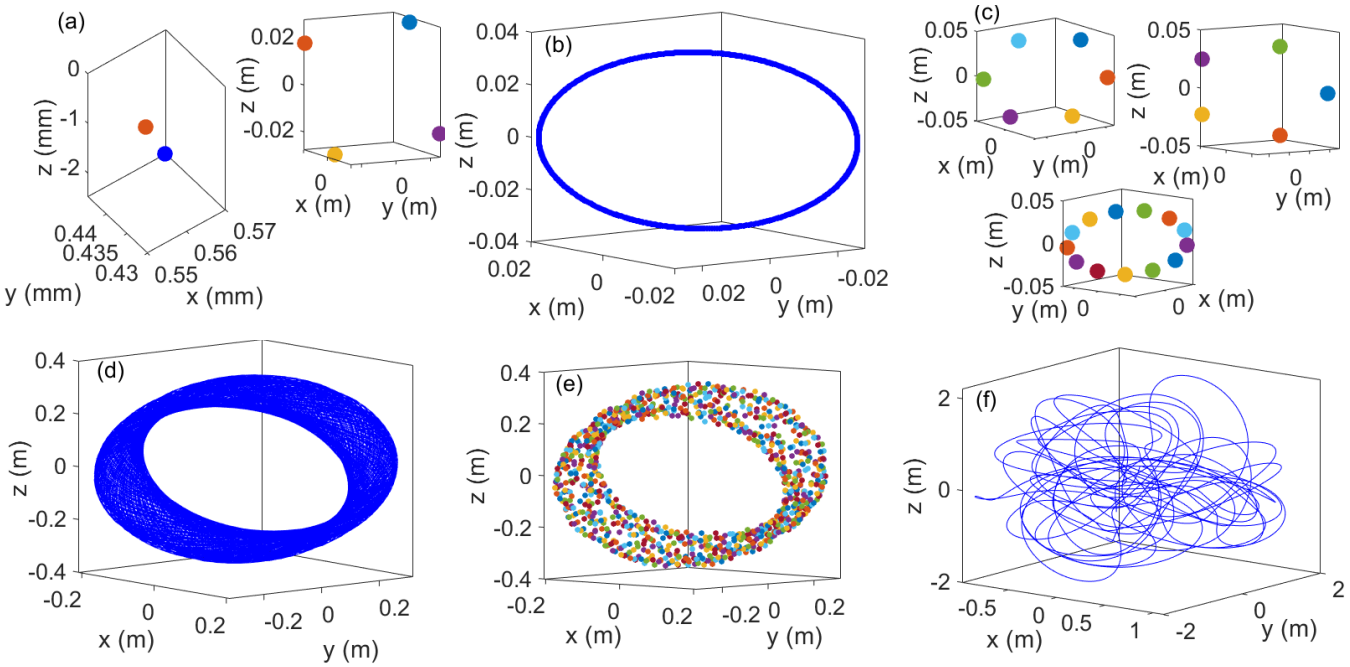

FIG. 1: Center of mass trajectories of different attractors for $N = 128$, $R_0 = v_0 = 1$, $\eta = 0$ and different β. **(a)** Period 2 ($\beta = 600$) and period 4 ($\beta = 300$) attractors. **(b)** Quasiperiodic attractor that appears at $\beta = 2N = 256$. **(c)** Periodic solutions with larger periods: 5 ($\beta \approx 177$), 6 ($\beta = N = 128$), and 13 ($\beta \approx 225$). **(d)-(e)** Torus-like chaotic attractor for $\beta = 1$ depicted for a long and a shorter time interval. **(f)** Chaotic attractor for $\beta = 0.01$: the center-of-mass trajectory will fill a sphere-like body if depicted for much longer times. Note that increasing β confines the motion to smaller volumes, from meters to millimeters.

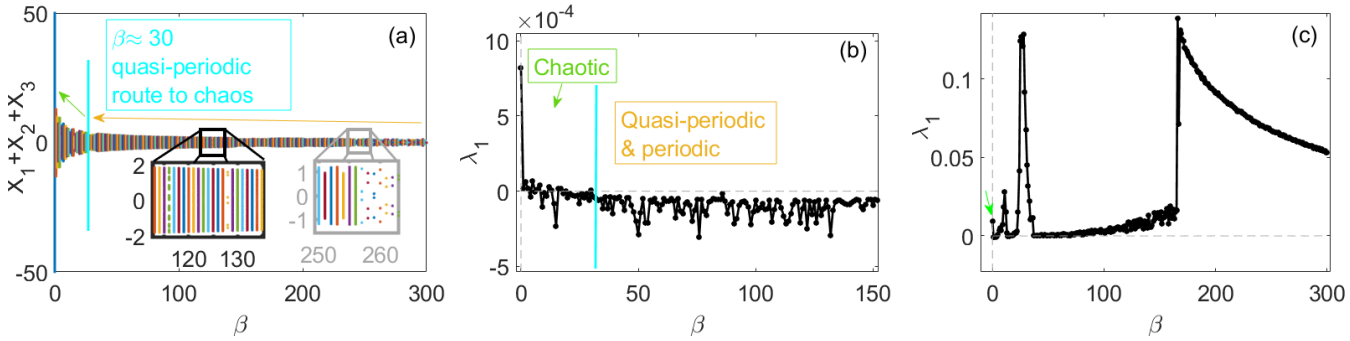

FIG. 2: **(a)** Bifurcation diagram of the sum of CM coordinates in nondimensional units and **(b)** largest Lyapunov exponent versus β for $\eta = 0$. The boxes in Panel (a) about $\beta = N$ and $\beta = 2N$ correspond to period 6 solutions and others interspersed with quasiperiodic solutions, and a period 4 to quasiperiodic transition, respectively. Chaotic solutions appear following the quasiperiodic route to chaos. Note the large increase of the interval of CM values as β decreases. **(c)** Same as Panel (b) for $\eta = 0.5$. Note how noise increases the value of the LLE and induces chaos for confinement values that correspond to quasiperiodic attractors for $\eta = 0$. The area marked by green arrow in Panel (c) corresponds to the scale-free chaos transitions discussed in the present paper. Other parameters are as in Fig. 1.

to assess the role of noise. As explained in Appendix B, three methods to calculate the LLE produce the same values and yield complementary information: (i) applying the Benettin algorithm to Eq. (1)[21–23]; (ii) using the Gao-Zheng test[24] on time traces of the swarm center-of-mass (CM) motion $\mathbf{X}(t)$ (which could be acquired from measurements of natural swarms); (iii) scale-dependent Lyapunov exponents from time traces, which discriminate between chaos and noise[25].

Fig. 3(a) is the phase diagram (η, β) displaying phases of deterministic, noisy chaos and noise. Inside the noisy chaos phase we have indicated the critical lines of scale-free chaos for different N. To distinguish chaotic and noise phases, we have plotted in Fig. 3(b) the scale-dependent Lyapunov exponent (SDLE) $\lambda(\varepsilon)$ calculated in Appendix B from time traces of center-of-mass motion with two-dimensional lagged vectors $m = 2$.[25] For $\eta = 0$, $\lambda(\varepsilon)$ is flat at small scale and de-

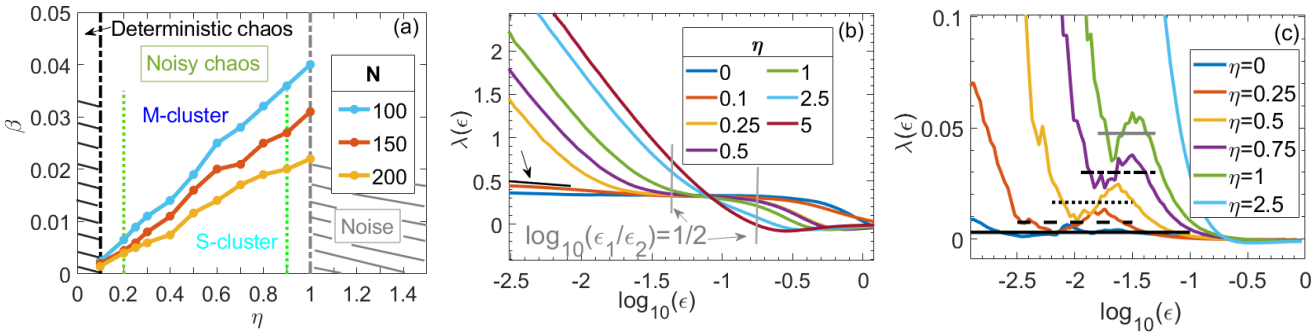

FIG. 3: **Scale-free chaos. (a)** Phase diagram β vs η exhibiting regions of deterministic and noisy chaos, and of noisy disorder. The vertical lines at $\eta = 0.2$ and 0.9 correspond to the maximum correlation length observed in experiments and to the noise for which the dynamic correlation function ceases to be flat near $t = 0$, respectively. Noise swamps chaos for $\eta \geq 1$. The three lines of critical points in the noisy chaos region correspond to critical confinement $\beta_c(N,\eta)$ for $N = 100, 150, 200$. **(b)** Largest scale-dependent Lyapunov exponent as a function of the scale parameter ε for $N = 100$, different values of η, two lagged coordinates $m = 2$ and $\beta = \beta_c(N,\eta)$, see Appendix B. The vertical lines mark the width of the critical plateau: $\log_{10}(\varepsilon_2/\varepsilon_1) = 1/2$ and correspond to the vertical dot-dashed lines in Panel (a). **(c)** Largest scale-dependent Lyapunov exponent as a function of the scale parameter ε for $N = 100$, different values of η, and $\beta = \beta_c(N,\eta)$ with $m = 6$, instead of $m = 2$ as in Panel (b). The averages of the oscillations corresponding to the plateau region in Panel (b) increase with the noise η indicating that so does the LLE: $\lambda_1(0) \sim 0.003, \lambda_1(0.25) \sim 0.0075, \lambda_1(0.5) \sim 0.0165, \lambda_1(0.75) \sim 0.03, \lambda_1(1) \sim 0.0476$.

creases for $\varepsilon \approx 1$. For nonzero noise, $\lambda(\varepsilon)$ decreases, reaches a plateau and decreases again as the scale ε increases. As noise increases, the curves $\lambda(\varepsilon)$ permit distinguishing regions in the phase plane (η,β) of Fig. 3(a) where chaos is either mostly deterministic, substantially altered or even induced by noise (noisy chaos), and swamped by noise[25]. The noise level used in the numerical simulations of Refs. 11–13 is 5.65 in our units. Thus, it is fully inside the noise region of Fig. 3(a), far from the noisy chaos parameter values we consider here.

When two lagged coordinates are sufficient to reconstruct the chaotic attractor from CM data, the value of the SDLE $\lambda(\varepsilon)$ at the plateau coincides with the LLE calculated directly from Eq. (1). This occurs for the Lorentz or Rossler attractors, as explained in Ref. 25. However, to reconstruct safely a chaotic attractor, the dimension of the lagged vectors should surpass twice the fractal dimension D_0.[22,23] For the VM, we have found that properly reconstructing the chaotic attractor requires at least 6 lagged coordinates. Six-dimensional CM trajectories contain self-intersections in dimension 2. Fig. 3(c) shows that the SDLE $\lambda(\varepsilon)$ with $m = 6$ displays oscillations for different noise values, not a single plateau as in Fig. 3(b). Thus, we need a different algorithm to calculate the LLE from data. We have used the Gao-Zheng algorithm[24] that requires constructing a quantity $\Lambda(k)$ whose slope near the origin produces the LLE, see Appendix B. These LLE yield the horizontal lines in Fig. 3(c), which coincide with the average values of the SDLE oscillations. The latter coincide with LLE calculated from Eq. (1) and increase with noise. Thus, noise enhances chaos in the noisy chaos region of Fig. 3(a), which includes critical lines of scale-free-chaos phase transitions, $\beta = \beta_c(N,\eta)$, to be explained in Section IV. Numerical evidence for $100 \leq N \leq 5000$ suggests that these lines move to $\beta = 0$ as $N \to \infty$. Without confinement, the LLE vanishes and chaos disappears. This is corroborated by a different argument.[26] The correlation length ξ is bound by the finite velocity of propagation c multiplied by the time it takes two points to move exponentially far from each other, i.e., $1/\lambda_1$:

$$\xi \leq \frac{c}{\lambda_1}. \tag{2}$$

Thus, a phase transition with infinite correlation length can only occur for $\lambda_1 = 0$.[26,27]

IV. PHASE TRANSITIONS WITHIN REGIONS OF CHAOS

Insect swarms are peculiar in that their polarization order parameter is small but they exhibit strong correlations.[11,12] We shall show later that the confined VM displays the same behavior near scale-free-chaos phase transitions. Cavagna *et al* have used data extracted from observations of natural swarms to calculate static and dynamic correlation functions and found power law behavior for susceptibility, correlation length and the dynamic correlation function[11–13]. Their work indicates that the Fourier transform of the dynamic connected correlation function (DCCF) is the key tool to find power laws and critical exponents[6,13]:

$$\hat{C}(k,t) = \left\langle \frac{1}{N} \sum_{i,j=1}^{N} \frac{\sin(k r_{ij}(t_0,t))}{k r_{ij}(t_0,t)} \delta\hat{\mathbf{v}}_i(t_0) \cdot \delta\hat{\mathbf{v}}_j(t_0+t) \right\rangle_{t_0} \tag{3}$$

Here k, $r_{ij}(t_0,t)$, $\mathbf{V}$, $\delta\mathbf{v}_i = \mathbf{v}_i - \mathbf{V}$, $\delta\hat{\mathbf{v}}_i = \delta\mathbf{v}_i / \sqrt{\frac{1}{N}\sum_j |\delta\mathbf{v}_j|^2}$ are the wavenumber, the distance between particles i and j at different times (particle positions are calculated in the center of mass reference frame), the center of mass velocity, the relative velocity, and the dimensionless velocity fluctuation of the

ith particle, respectively. The brackets in (3) indicate an average over the earlier time t_0 and an ensemble average over random initial conditions[13]. See Appendix C for details.

For natural swarms and their numerical simulations, conservation of the number of particles requires adapting the statistical mechanics definitions of correlation functions, correlation length and susceptibility[7,15], as discussed in Ref. 6. The equilibrium static connected correlation function (SCCF) $\hat{C}(k,0)$ reaches a maximum at $k=0$, which is the susceptibility. However, $\hat{C}(0,0)=0$ and, for finite N and near a phase transition, $\hat{C}(k,0)$ reaches a maximum at a critical wavenumber k_c. This maximum is the susceptibility χ, which tends to infinity as $N\to\infty$ at the critical confinement.[6] The FSS hypothesis implies that $k_c\xi$ (ξ is the correlation length) is a number of order 1 and a possible choice is $\xi = 1/k_c$.[6] How do we obtain the critical confinement $\beta_c(N,\eta)$? From the theory of equilibrium phase transitions, we would expect: (i) the maximum and the inflection point of the SCCF versus β tend to infinity as $N\to\infty$ for fixed alignment noise; (ii) the correlation (relaxation) time of the DCCF at wavenumber k_c tends to infinity as $N\to\infty$ (critical slowing down). We will use these criteria to identify lines of phase transitions in the chaotic phases of the confined VM.

A. Critical confinement from correlation time

For the DCCF, the dynamic scaling hypothesis implies

$$\frac{\hat{C}(k,t)}{\hat{C}(k,0)} = f\left(\frac{t}{\tau_k}, k\xi\right) = g(k^z t, k\xi); \quad g(t) = \frac{\hat{C}(k_c,t)}{\hat{C}(k_c,0)}, \quad (4)$$

with $k_c = \text{argmax}_k \hat{C}(k,t)$. Here z is the dynamic critical exponent and $\tau_k = k^{-z}\phi(k\xi)$ is the correlation time of the NDCCF (4) at wavenumber k obtained by solving the equation:[13,14]

$$\sum_{t=0}^{t_{max}} \frac{1}{t}\sin\left(\frac{t}{\tau_k}\right) f\left(\frac{t}{\tau_k}, k\xi\right) = \frac{\pi}{4}, \quad (5)$$

where t_{max} is the maximum time in experiments or in VM simulations[13]. For pure exponential relaxation, Eq. (5) equals the relaxation time, whereas for pure oscillation, Eq. (5) gives the oscillation period.[13,14] The NDCCF of a chaotic attractor first relaxes rapidly and then it exhibits damped oscillations as time elapses, cf. Fig. 4. The rapid relaxation of $g(t)$ at short times is reminiscent of behavior near equilibrium phase transitions captured by Eq. (5). Thus, to describe the short-time relaxation at $k_c \sim 1/\xi$, we should find the minimum relaxation time from Eq. (5) with $k = k_c$. By critical slowing down, this minimum goes to infinity as $N\to\infty$. To capture the shortest time scales within critical slowing down, we define the critical confinement $\beta_c(N,\eta)$ as the value of β (for fixed N and η) at which τ_k reaches its minimum value for $k = k_c$.

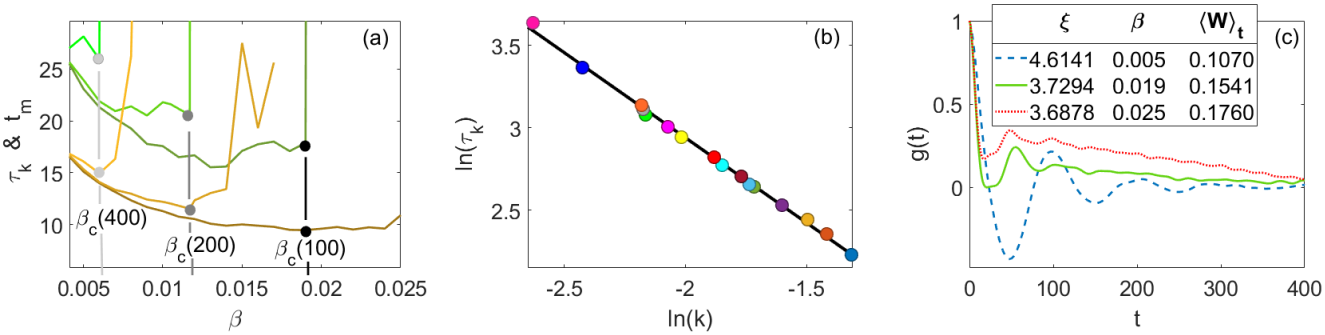

FIG. 4: **(a)** Smallest time $t_m(\beta;N)$ such that $g(t_m)=0$ (green curves) and characteristic timescale $\text{argmin}_\beta \tau_{k_c}(\beta;N)$ (brown curves) as functions of β for $N = 100, 200, 400$ (darker to lighter colors). The minimum characteristic timescale is close to the abrupt growth of $t_m(\beta;N)$ and marks the scale-free-chaos phase transition. **(b)** Characteristic timescale, τ_k, computed at $k_c = 1/\xi$ for different N, as a function of k (log-log scale): $\tau_{k_c} \sim k_c^{-z}$ with $z = 1.01 \pm 0.01$. **(c)** Normalized DCCF vs nondimensional time for different confinement values and $N = 100$. In this figure, $\eta = 0.5$.

Fig. 4(a) displays the smallest time $t_m(\beta,N)$ at which $\hat{C}(k_c,t)=0$ and the correlation time τ_{k_c} as functions of β for $N = 100, 200, 400$. For the wavenumber $k_c = 1/\xi$, t_m and τ_k reach their minima at very close values of β. In particular, at β slightly larger than β_c, the first local minimum of $\hat{C}(k_c,t)$ becomes positive and the minimum t_m having $\hat{C}(k_c,t)=0$ jumps to a much larger value, cf. Fig. 4(a). As $N\to\infty$, $\beta_c\to 0$ and the characteristic timescale tends to infinity (critical slowing down). The NDCCF $g(t)$ oscillates with time as shown in Fig. 4(c) for $N = 100$. When $\beta < \beta_c$, $g(t)$ has different zeros and minima at negative values. At $\beta_c(N,\eta)$, the first minimum crosses the horizontal axis and $g(t)$ reaches the next zero for

much larger times. This corresponds to the vertical green line in Fig. 4(a) for $N = 100$. Fig. 4(c) shows that $g(t)$ first vanishes at a larger time when $\beta > \beta_c(N,\eta)$.

Experimental data suggest that setting $k_c\xi = 1$ and choosing an appropriate value of z collapse $\hat{C}(k,t)/\hat{C}(k,0)$ into a single function of $k^z t$ with $z = 1.12 \pm 0.16$.[13] Our numerical simulations of the confined VM yield a power law $\tau_{k_c} \sim k_c^{-z}$ with $z = 1$ ($z = 1.01 \pm 0.01$), as indicated in Fig. 4(b). Fig. 5 illustrates how NDCCF curves collapse to a single one in terms of $k_c^z t$ at the scale-free chaos line for $0 < k_c^z t < 4$ provided $z = 1.01 \pm 0.01$. Moreover, NDCCF curves drop to values close to zero for $k^z t > 5$ but they do not collapse for those larger times.

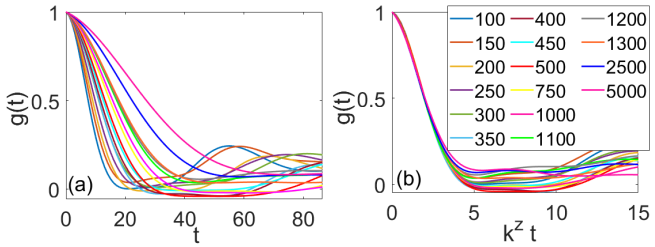

FIG. 5: Dynamic scaling of the NDCCF. $g(t)$ versus **(a)** t, and **(b)** $k^z t$, for the different values of N listed in the inset and $z \approx 1$. Here $\eta = 0.5$.

Having found the critical confinement $\beta_c(N;\eta)$, we can find the power laws and the critical exponents for the correlation length, susceptibility and the LLE λ_1 in terms of $\beta = \beta_c(N;\eta)$:

$$\chi(\beta,N,\eta) \equiv \max_r Q(r) \sim \beta^{-\gamma},\ \xi \equiv \text{argmax}_r Q(r) \sim \beta^{-\nu}, \quad (6)$$

$$\lambda_1 \sim \beta^{\varphi} \sim N^{-\frac{\varphi}{3\nu}}, \quad (7)$$

as $\beta = \beta_c(N;\eta) \to 0$ with $N \gg 1$. To calculate the susceptibility, we have used the maximum of the cumulative real-space correlation function (corresponding to the first zero r_0 of the real-space correlation function) at $\beta_c(N;\eta)$:

$$Q(r) = \frac{1}{N}\sum_{i=1}^{N}\sum_{j\neq i}^{N} \delta\hat{\mathbf{v}}_i \cdot \delta\hat{\mathbf{v}}_j \theta(r - r_{ij}), \quad (8)$$

where $\theta(x)$ is the Heaviside unit step function and this correlation length is the first zero r_0 of the real-space SCCF.[11,12] As shown in Appendix C, selecting $\hat{C}(k_c,0)$ as the susceptibility does not produce a monotonic function of β_c or of N. Thus, $\hat{C}(k_c,0)$ cannot be used to fit a power law over an extended range. However, $1/k_c$ and r_0 are linearly related, and using either one as correlation length yields the same critical exponent ν; see Appendix C. A similar relation between $1/k_c$ and r_0 also holds for midge data; see Fig. SF1 of Ref. 13. To calculate the LLE we can use the Benettin algorithm for the VM of Eq. (1) or a convenient time series obtained from the simulations, e.g., the CM evolution or the NDCCF; see Appendix B.

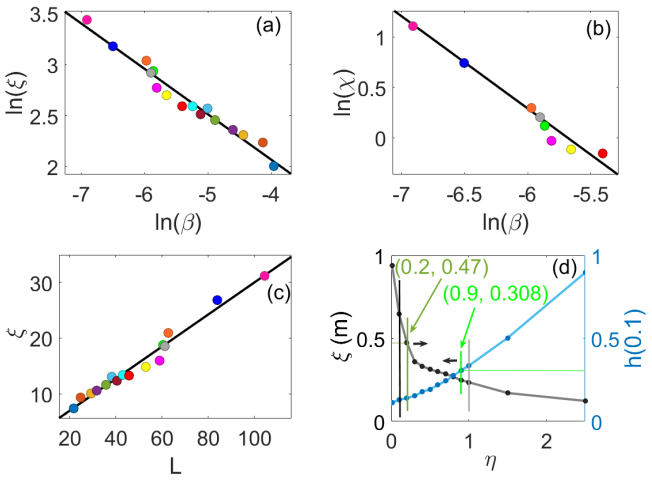

FIG. 6: **(a)** Scaling of the dimensionless correlation length with β (log-log scale): $\xi \sim \beta^{-\nu}$ with $\nu = 0.436 \pm 0.009$. **(b)** Scaling of the real-space susceptibility with β (log-log scale): $\chi \sim \beta^{-\gamma}$ with $\gamma = 0.92 \pm 0.05$ for $N = 500$, 750, 1000, 1100, 1200, 1300, 2500, 5000. **(c)** The correlation length increases linearly with L. **(d)** Correlation length (in meters) $\xi = r_0$ and NDCCF flatness $h(0.1)$ vs noise. Black vertical bars delimit the region of noisy chaos, which occurs for smaller noise values than the order-disorder flocking transition[11–13]. Green vertical bars are compatible with observations of natural swarms: the leftmost bar marks the largest observed correlation length and the rightmost bar marks when NDCCF flatness ends. Here $\eta = 0.5$. In Panels (a) and (c), N values are as in Fig. 5(b).

Figs. 6(a) and 6(b) depict how correlation length and real-space susceptibility scale with β and Fig. 6(c) confirms that the correlation length is proportional to the linear size of the swarm. For $\eta = 0.5$, we obtain the critical exponents $\nu = 0.436 \pm 0.009$ and $\gamma = 0.92 \pm 0.05$, respectively. Fig. 6(d) shows that the correlation length (in meters) decreases with alignment noise at critical confinement. Correlation length values in the region of noisy chaos are compatible with observations of natural swarms[11–13].

The LLE λ_1 decreases as $\beta_c(N;\eta)$ does according to the power law (7) with critical exponent $\varphi = 0.43 \pm 0.03$ provided the LLE is calculated using the Benettin algorithm on Eq. (1) or time traces of the CM as explained in Appendix B. See Fig. 7(a). For chaotic systems with short range interactions such as the confined VM, Eq. (2) together with Eqs. (6) and (7) imply that $\beta^{\varphi-\nu} \leq c$. To be consistent as $\beta \to 0$, this relation then implies

$$\varphi \geq \nu. \quad (9)$$

Were the dynamic scaling of (4) to hold for all time, $e^{\lambda_1 t}$ would be a function of $k^z t$; therefore $\lambda_1 \sim k_c^z \sim \beta^{z\nu}$, and $\varphi = z\nu$. Eq. (9) then produces $z \geq 1$, which agrees with all our simulations carried out with the Benettin algorithm or reconstructing the chaotic attractor from center of mass data. Thus, $\varphi \approx z\nu \geq \nu$ approximately holds for one-time functions such as the center of mass trajectory with $\eta = 0.5$. However, this

relation fails for the two-time NDCCF, which has a smaller φ; see Fig. 7(a).

Remarkably, our calculations cast light on an unexplained feature of swarm data. The NDCCF in Fig. 5(b) collapses to a single curve for small values $0 < k^z t < 4$ but not for larger values. The same two features are observed in midges, Fig. 2b of Ref. 13, but cannot be explained by the order-disorder phase transition of the Vicsek model, Fig. 2e of Ref. 13. *What happens?* Fig. 7(b) shows that the box-counting dimension D_0 and D_q for $q > 0$ undergo a downward trend with increasing N (decreasing β). Then the dimension of the more commonly visited sites of the attractor decreases. Furthermore, (7) indicates that the positive LLE tends to zero and chaos disappears as $\beta \to 0$, but the chaotic attractor remains multifractal: different time scales persist[23]. Thus, a single rescaling of time as in Fig. 5(b) cannot collapse the full NDCCF, either in our simulations or in observations of natural swarms.

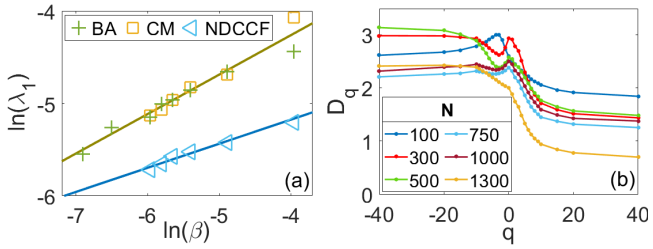

FIG. 7: **(a)** LLE vs β for different N, $\lambda_1 \sim \beta^{\varphi}$, calculated by the Benettin algorithm[21] for the complete system (crosses), from CM motion (squares) and from the NDCCF (triangles). We get $\varphi = 0.43 \pm 0.03$ (crosses and squares), and $\varphi = 0.24 \pm 0.02$ (triangles). **(b)** Multifractal dimension[23] D_q vs q at $\beta_c(N;0.5)$.

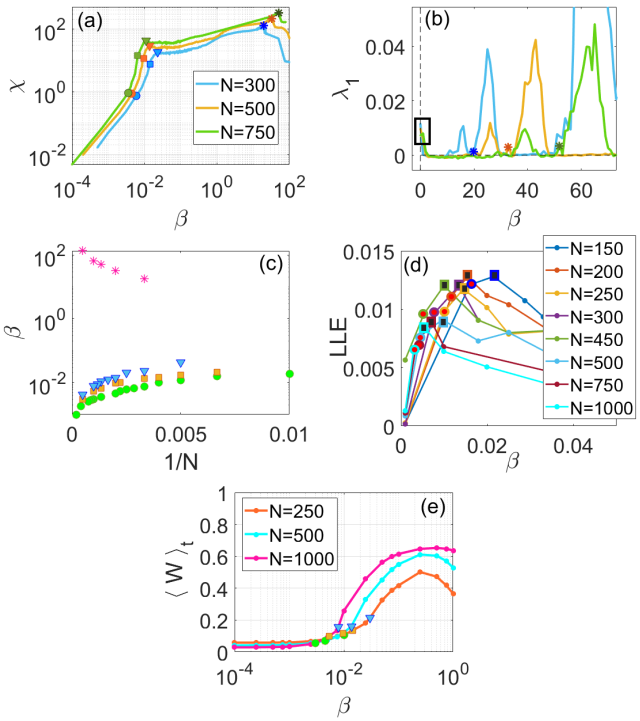

FIG. 8: **(a)** Real-space susceptibility (log-log scale) and **(b)** LLE versus β for $N = 300, 500, 750$. Circles, squares, triangles and asterisks mark β_c, β_i, β_m (local χ maximum), and β_M (global χ maximum of the susceptibility), respectively. **(c)** β_c, β_i, β_m, and β_M versus $1/N$. **(d)** LLE versus β for N marked in the inset. **(e)** Time averaged polarization versus β. Circles correspond to the critical confinement $\beta_c(N;\eta)$, squares correspond to the inflection point of the susceptibility $\beta_i(N;\eta)$. Here $\eta = 0.5$.

Another feature shared by swarm data and the scale-free-chaos phase transition is that the NDCCF is flat at small times. Referred to (4), we define 'flatness' as

$$h(x) = -\frac{1}{x}\ln f(x,1), \quad x = \frac{t}{\tau_k}. \tag{10}$$

Perfectly flat supposes $h(0) = 0$. However, measuring $h(0)$ in insect swarms is not practical because $h(x)$ changes abruptly below $x = 0.1$, as Fig. 3b of Ref. 13 shows. The same figure yields an upper value 0.3 of $h(0.1)$ for natural swarms, which we select as the transition value from flat to non-flat NDCCF. At the VM order-disorder phase transition, $h(0.1) \approx 1 > 0.3$ (exponential decay, clearly non-flat NDCCF)[13]. For the confined VM, the transition value occurs at $\eta = 0.9$ in Fig. 6(d) and in Fig. 3(a), which is close to the change to noise from noisy chaos at $\eta = 1$ (lower than the noise for order-disorder phase transition)[11–13]. As noise increases, Fig. 6(d) shows that the correlation length decreases and $h(0.1)$ increases. Thus, observed correlation lengths and flat NDCCFs occur in the region of noisy chaos that contains the scale-free-chaos phase transitions.

B. Critical confinement from the static correlation

At critical confinement, the susceptibility $\chi = \max_r Q(r)$ given by Eqs. (6) and (8) for fixed $\beta_c(N;\eta)$, η and N becomes infinity as $N \to \infty$. For given values of the alignment noise η, we can find other values of β, e.g., the local maximum and the inflection point of $\chi = \chi(\beta, N;\eta)$ as a function of β, which also tend to infinity as $N \to \infty$. At finite N, these confinement values, $\beta_i(N;\eta)$ (inflection) and $\beta_m(N;\eta)$ (local maximum), are different from $\beta_c(N;\eta)$, as shown in Fig. 8(a). Fig. 8(b) illustrates that the susceptibility global maximum is reached at large values of β corresponding to the second chaotic window, which is different from the scale-free chaos window of β_c, β_i, β_m. Unlike the isolated β_M, the values β_c, β_i and β_m tend to 0 as $N \to \infty$, as observed in Fig. 8(c). These lines produce the same critical exponent for the correlation length (see below) and therefore they correspond to the same line of phase transitions. Fig. 8(d) shows that the LLE versus β curve reaches a local maximum at β_i. Thus, maximum 'chaoticity' is reached at the line of susceptibility inflection points. The LLE power law of Eq. (7), calculated from Eq. (1), has a critical exponent $\varphi_i = 0.33 \pm 0.04$ at $\beta = \beta_i$, and $z_i \nu_i \approx 0.66 > \varphi_i$.

Fig. 8(e) shows the average polarization as a function of $\ln\beta$ for $N = 250, 500, 1000$. As N increases, β_c, β_i, β_m decrease to zero and so do the corresponding polarization order parameter, which suggest that these lines represent second order phase transitions.

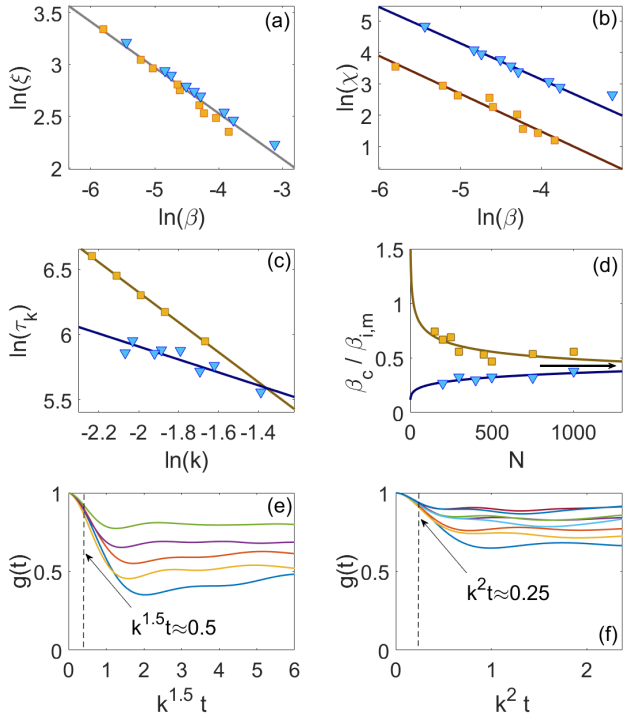

FIG. 9: Power laws of **(a)** dimensionless correlation length and **(b)** real-space susceptibility versus $\beta_i(N;\eta)$ (inflection point) and $\beta_m(N;\eta)$ (local maximum of χ) for $150 \le N \le 2000$. Critical exponents are $\nu_{i,m} = 0.44 \pm 0.02$ (all points), $\gamma_i = 1.20 \pm 0.09$, and $\gamma_m = 1.15 \pm 0.03$, respectively. **(c)** Scaling of the correlation time at the inflection point and at the local maximum: $\tau_k \sim k_c^{-z_{i,m}}$, $z_i = 1.15 \pm 0.02$, $z_m = 0.50 \pm 0.09$, respectively. **(d)** Ratios $\beta_c/\beta_i \sim 0.47$ and $\beta_c/\beta_m \sim 0.37$ as $N \gg 1$. Collapse of NDCCF data as function of **(e)** $k^{1.5}t$ at the inflection point and of **(f)** $k^2 t$ at the local maximum of the susceptibility on the indicated narrow interval near $t = 0$. Here $\eta = 0.5$ and squares and triangles correspond to β_i and β_m, respectively.

Figs. 9 depict power laws for correlation length, time and collapse of the NDCCF at the lines β_i and β_m, which merge with β_c as $N \to \infty$. At critical confinement given by the susceptibility inflection point $\beta_i(N;\eta)$ and $\beta_m(N;\eta)$, there is finite size scaling with critical exponents $\nu_{i,m} = 0.44 \pm 0.02$ (correlation length) and $\gamma_i = 1.20 \pm 0.09$, $\gamma_m = 1.15 \pm 0.03$, cf Figs. 9(a) and 9(b). Notice that $\gamma_i = \gamma_m$ within error estimates. The critical exponent ν is the same (within the error estimate) as calculated for the critical line $\beta_c(N;\eta)$, whereas the exponents γ are somewhat larger (0.92 versus 1.15). The dynamic critical exponents calculated from Eq. (5) in Fig. 9(c), $z_i = 1.15$ and $z_m = 0.50$ are unreliable as NDCCF data do not collapse for these values. Instead, the NDCCF collapse for $z_i = 1.5$ on $0 < k^z t < 0.5$ and $z_m = 2$ on $0 < k^z t < 0.25$, as shown in Fig. 9(e) and 9(f). Furthermore, the minima of $g(t)$ are all larger than 0.3, hence they are no longer close to zero as in Fig. 5. We conclude that Eq (5) can only be used for the transition from single cluster to muticluster chaos at β_c.

The ratios β_c/β_i and β_c/β_m are displayed in Fig. 9(d), which suggests they become constant (about 0.47 and 0.37, respectively) as $N \to \infty$. As the critical exponent ν is the same, β_c, β_i, β_m scale as $N^{-1/(3\nu)}$. This argument, together with Fig. 8(c), suggest that the three lines $\beta_c(N;\eta) < \beta_i(N;\eta) < \beta_m(N;\eta)$ converge to zero as $N \to \infty$ at the same rate. However, these lines have different critical exponents γ and z: while $\gamma_i \approx \gamma_m$, the dynamical critical exponents $z_i = 1.5$, $z_m = 2$ are different and larger than $z = 1$ obtained for β_c. Do the lines $\beta_c(N;\eta)$, $\beta_i(N;\eta)$, and $\beta_m(N;\eta)$ describe ultimately the same phase transition? Answering satisfactorily this question requires hard mathematical analysis (not just numerical simulations), which we are far from being able to provide at the present time. However, we can say this. That the lines $\beta_i(N;\eta)$ and $\beta_m(N;\eta)$ (inflection point and local maximum of the susceptibility) correspond to the same phase transition seems evident. Numerical simulations indicate that the power laws associated to these lines have essentially the same values of γ and ν, while their different values of z may just indicate different time scales involved in the same transition. The single cluster to multicluster critical line has the smaller value of β for finite N and it has consistent critical exponents as calculated using all Eqs. (5)-(8). The correlation time of Eq. (5) produces the wrong critical dynamical exponents for $\beta_i(N;\eta)$ and $\beta_m(N;\eta)$. If the lines $\beta_c(N;\eta)$ represent a different phase transition from that of $\beta_i(N;\eta)$ and $\beta_m(N;\eta)$ as $N \to \infty$, then scale-free chaos and power laws extend beyond $\beta_c(N;\eta)$ (albeit to lines in a region that vanishes as $N \to \infty$ and all β tend to 0). If there is a sole phase transition for each value of η, then the different values of the exponents γ are somewhat puzzling. They could be associated to different length scales in the multifractal chaotic dynamics at the three critical lines. The connection between dynamics and susceptibility in nonequilibrium phase transitions needs further study.

C. Critical exponents and observations

We have found a line of phase transitions $\beta_c(N;\eta)$ representing the change from scale-free single to multicluster chaos. For $\eta = 0.5$ (middle of the noisy chaos region), as $\beta = \beta_c(N;\eta) \to 0$, $N \to \infty$, we have obtained $\nu = 0.436 \pm 0.009$ (correlation length), $\gamma = 0.92 \pm 0.05$ (real-space susceptibility), and $z = 1.01 \pm 0.01$ (dynamic exponent). The critical exponent for the LLE law is approximately $\varphi = z\nu$. The critical exponents change little for $0.1 < \eta < 1$.

In observations of natural swarms, the measured critical exponents are $\nu = 0.35 \pm 0.10$, $\gamma = 0.9 \pm 0.2$ (Ref. 11 and 12), and $z = 1.12 \pm 0.16$ (Ref. 13), while the real-space susceptibility is between 0.32 and 5.57 for the measured swarms.[11,12] It is important to note that the average velocity is defined differently in Refs. 12 and 13. In Ref. 13, the average veloc-

ity is defined as the velocity of the center of mass $\mathbf{V}$, Eq. (3) and Appendix C. However, overall rotations and dilations are subtracted from $\mathbf{V}$ in Refs. 11 and 12. Thus, while we can compare directly our dynamical critical exponent with observations, our exponents ν and γ do not involve the rotations and dilations used in the calculations of Ref. 12. This remark notwithstanding, the observed critical exponents are compatible with those calculated near the critical confinement based on correlation time, cf Fig. 6 (γ and z values corresponding to β_i or β_m are larger and differ appreciably from experimental observations while ν is the same). On the other hand, swarm critical exponents calculated in the literature (based on the order-disorder phase transition) are widely off the mark: $\gamma = 1.6 \pm 0.1$, $\nu = 0.75 \pm 0.02$ (Ref. 12), $z = 1.5$ (Refs. 29 and 30). Even for the two-dimensional Vicsek model at the order-disorder phase transition,[31] $z = 1.27$.

Recently, Holubec *et al* have studied the VM with time delay and periodic boundary conditions. They found $\gamma \approx 1.53$, $\nu \approx 0.75$ (larger than measured in midges) and $z \approx 1$ for very long delay times using an undersampled NDCCF[32]. Their NDCCF exhibits regular oscillations as the time delay increases, which are interpreted using a time-delayed reaction-diffusion equation (see Supplementary Information in Ref. 32). It is not clear whether there is a single phase transition responsible for these results. In time-delayed ordinary differential equations, oscillations often appear as Hopf bifurcations at critical delays[33] and may evolve to relaxation oscillations as delays increase[34]. Delayed reaction-diffusion equations can have stable relaxation-type wavetrain solutions that depend on the variable $(x+ct)$, cf Ref. 34. This would give a dynamic exponent $z = 1$. Further study of the time-delayed VM may shed light on these connections.

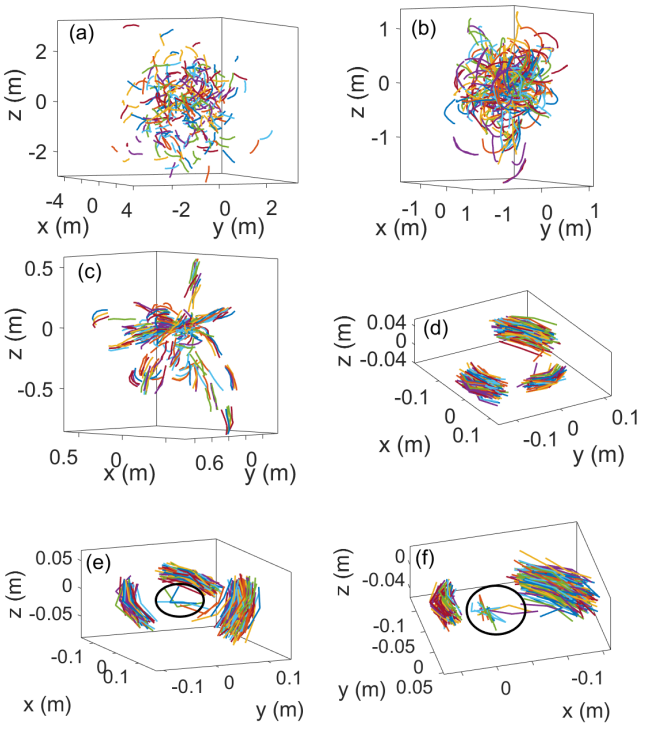

FIG. 10: Chaotic swarms of $N = 300$ particles showing short trajectories of the particles for confinements near its critical value, $\beta = \beta_c(N;\eta)$ and $\eta = 0.5$: **(a)** Sparse single cluster chaos for $\beta < \beta_c(N;\eta)$, **(b)** compact single cluster chaos at $\beta = \beta_c(N;\eta)$, multicluster chaos for **(c)** $\beta > \beta_c(N;\eta)$ and for **(d)** $\beta = \text{argmax}\ \chi(\beta) = 19.8$. **(e)** For $\beta = 21$, three chaotic clusters move around a central sphere (located by a black circle) where other particles are confined; and **(f)** for $\beta = 25$, only two chaotic clusters remain and more particles are trapped in the central sphere. Unit of length is 1 meter.

V. PHASE TRANSITION AND TOPOLOGICAL DATA ANALYSIS

The structure of clusters changes as β surpasses β_c, the critical confinement calculated from relaxation time. Fig. 10(a) shows the swarm particles and their short time trajectories for $\beta < \beta_c(N;\eta)$: the particles form a single cluster. Figs. 10(b) and 10(c) correspond to $\beta = \beta_c(N;\eta)$ and $\beta > \beta_c(N;\eta)$, respectively. For $\beta = \beta_c(N;\eta)$, the particles form a single cluster and fill a smaller volume, whereas for $\beta > \beta_c(N;\eta)$, the swarm has split in several clusters. Fig. 8(e) shows that the average polarization is very small for sparse single-cluster chaos, $\beta < \beta_c(N;\eta)$, and it increases with β in the multicluster chaotic region, $\beta > \beta_c(N;\eta)$. Multicluster behavior is even clearer when β gives the global maximum of the susceptibility as in Fig. 10(d). For larger values of β, some particles start being confined in a sphere centered at the origin and their number increases with β, as shown in Figs. 10(e) and 10(f).

These findings can be rendered more precise by *topological data analysis* (TDA)[35–37]. TDA borrows ideas from persistent homology, traditionally used to distinguish structures in low dimensional topological spaces (e.g., circle, annulus, sphere, torus, etc) by quantifying their connected components, topological circles, trapped volumes. For instance, given a point cloud $\mathbf{x}_1, \ldots, \mathbf{x}_N$ in $\mathbb{R}^3$, we can infer whether it represents a sphere or a torus by calculating the homologies H_0, H_1, H_2, and the corresponding Betti numbers b_0, b_1, b_2. The different homologies can be calculated regardless of the dimension of the underlying space, as long as a distance or metric is defined[35].

We consider midges (or particles) as data points from a sampling of the underlying topological space of the swarm. Thus, we have a finite set of data points from a sampling of the underlying topological space. We measure data homology by creating connections between nearby data points, varying the scale over which these connections are made (as given by the *filtration parameter*), and looking for features that persist across scales[35,36]. This can be achieved by building the *Vietoris-Rips complex* from all pairwise distances between points in the dataset. Assume spheres of diameter r circle each particle. For each value of the filtration parameter $r > 0$, we form a simplicial complex S_r by finding all gatherings of $k+1$ points such that all pairwise distances between these points are smaller than r. Each such gathering is a k-simplex. The simplicial complex S_r comprises finitely many simplices such

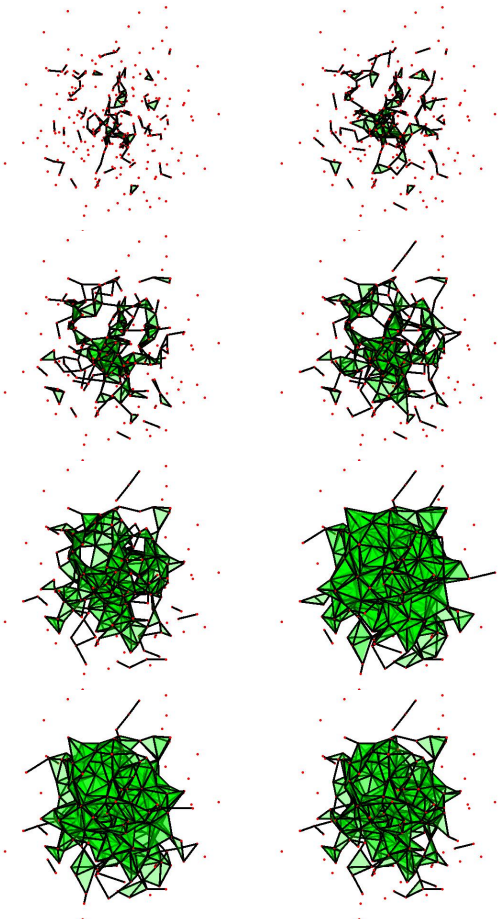

FIG. 11: Simplices for filtration values $r = \frac{r_M}{2}\tilde{r}$, $\tilde{r} = 0.05, 0.06, 0.07, 0.08, 0.09, 0.1, 0.11, 0.12$ at a representative time of the swarm evolution. Here $r_M = 150.22$ is the maximum distance between two points in the cloud, $\beta = 0.001 < \beta_c(300) = 0.0075$. As r increases, a single dominant cluster absorbs neighboring points and small components becoming a large 'compact' component.

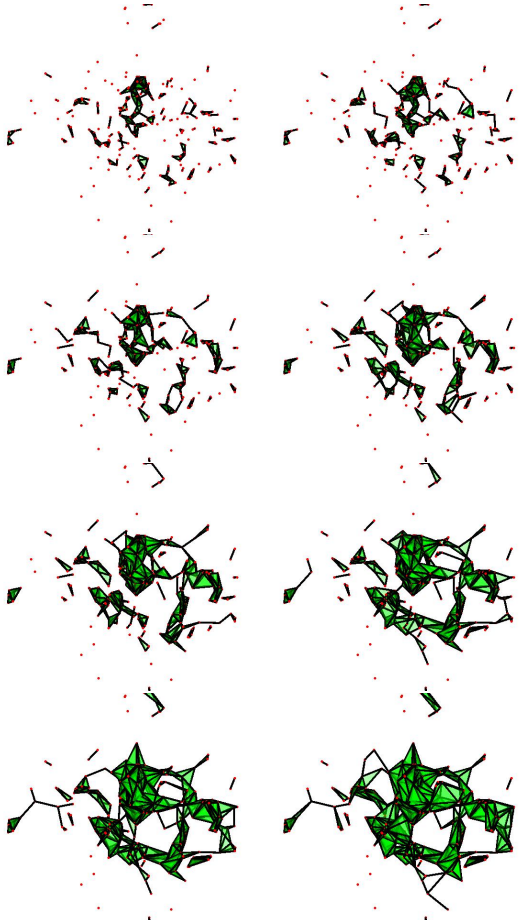

FIG. 12: Same as Fig. 11 for $\beta = 0.025 > \beta_c(300)$ with $r_M = 33.48$. As r increases, small separated components form and eventually connect leaving large holes.

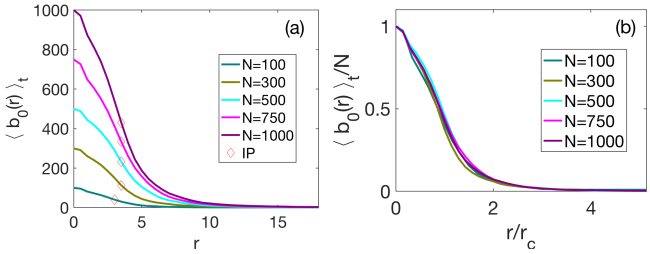

FIG. 13: **(a)** Time averaged Betti number $\langle b_0 \rangle_t$ versus filtration parameter r for $\beta_c(N;\eta)$ and different N; **(b)** Same for scaled averaged Betti number $\langle b_0 \rangle_t / N$ versus scaled filtration parameter r/r_c where $r_c(N)$ is the inflection point of each curve marked with diamonds in Panel (a). Here $\eta = 0.5$.

that (i) every nonempty subset of a simplex in S_r is also in S_r, and (ii) two k-simplices in S_r are either disjoint or intersect in a lower dimensional simplex. In S_r, 0-simplices are the data points, 1-simplices are edges, connections between two data points, 2-simplices are triangles formed by joining 3 data points through their edges, 3-simplices are tetrahedra, and so on. See Figs. 11 and 12, which are the counterparts of Figs. 10(a) and 10(c), respectively. These figures illustrate how TDA automatically characterizes the formation of a loose single swarm for $\beta < \beta_c$ and of several tight smaller clusters for $\beta > \beta_c$. In the latter case, the single cluster resulting for sufficiently large filtration parameter contains large holes.

To quantify the topological structure of the swarm data points, the Betti numbers depicted in Fig. 13 are useful. Within the set of all k-simplices in S_r, we can distinguish closed submanifolds called *k-cycles*, and cycles called *boundaries* because they are also the boundary of a submanifold. A *homology class* is an equivalence class of cycles modulo boundaries. A homology class H_k is the set of independent topological holes of dimension k, represented by cycles which are not the boundary of any submanifold. The dimension of H_k is the kth *Betti number* b_k. For instance, b_0 is the number of connected components shown in Fig. 13, b_1 is the number of topological circles, b_2 is the number of trapped volumes, and so on. See Refs. 35 and 36 for precise defini-

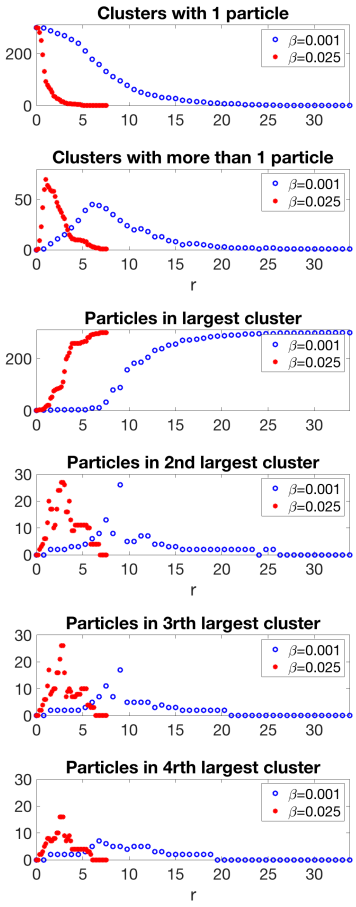

FIG. 14: Hierarchical TDA clustering. **(a)** Number of clusters with 1 particle (up) and with more than 1 particle (down) for $\beta = 0.025$ (left red points) and $\beta = 0.001$ (right blue points) vs filtration parameter r at a single time. **(b)** Number of particles in (up) the largest cluster and (down) the second largest cluster vs r. **(c)** Number of particles in (up) the third largest cluster and (down) the fourth largest cluster vs r. Here $N = 300$ and $\eta = 0.5$.

tions. At critical confinement, we can depict average Betti numbers, $\langle b_0 \rangle_t$ (number of connected clusters averaged over several time snapshots of the swarm), versus r for different N. These Betti numbers collapse when we rescale them using the inflection point of each curve[37], $r_c(N)$; see Figs. 13(a) and 13(b).

Fig. 14 illustrates the trend to a more compact single swarm and to swarm splitting as β increases past its critical value. As r increases, the number of clusters with a single particle decrease monotonically, as seen in the upper panel of Fig. 14(a). However, the upper panel of Fig. 14(b) shows that the number of particles in the largest cluster increase monotonically for $\beta < \beta_c$ but it increases with plateaus and abrupt jumps for $\beta > \beta_c$. These abrupt features indicate that the largest cluster absorbs single particles as r increases if $\beta < \beta_c$, whereas several large clusters form and are abruptly absorbed by the largest cluster at particular values of r for $\beta > \beta_c$. The lower panels in Figs. 14(a)-14(b) confirm these observations. Clusters with more than one particle form gradually if $\beta < \beta_c$ and abruptly if $\beta > \beta_c$. The plateaus and jumps in the number of particles within the second, third and fourth largest clusters in Figs. 14(b) and 14(c) indicate absorptions thereof by the largest cluster. These figures also illustrate the different cluster structure below and above the critical confinement β_c. When $\beta > \beta_c$, we observe the presence of several relevant clusters with a large number of particles. These clusters persist as the filtration parameter increases. Note that it is possible to have more than one cluster with the same number of particles.

VI. DISCUSSION AND CONCLUSIONS

The standard VM[17–20] confines particles in a box with periodic boundary conditions and is translationally invariant. Thus, it could describe the interior of a very large swarm that occupies a volume so large that boundaries do not influence its inner part. Natural midge swarms comprise hundreds of insects and form about a marker. Whether periodic boundary conditions properly describe them is questionable and it is not surprising that critical exponents based on the standard VM are different from observed ones.

We have discovered a line of phase transitions in the Vicsek model confined by a harmonic potential characterized by scale free chaos as confinement vanishes. More sophisticated confined VMs with anisotropic confinement potentials due to gravity[16] are worth exploring and may be closer to observations of natural swarms. However, the present work uncovers hitherto unexplored ground. To our knowledge, there is no previous work on scale-free-chaos phase transitions and we have used tools from dynamical systems and from statistical mechanics to describe them.

Let us start with dynamical systems tools. As the confinement strength decreases, the VM with fixed number of particles N displays a variety of periodic, quasiperiodic and chaotic attractors, which may be strongly modified by alignment noise. To distinguish chaos, we have calculated the largest Lyapunov exponent directly from the VM using the Benettin algorithm.[21] This is particularly well adapted to the discrete time dynamics of the VM. We have also calculated the LLE by reconstructing the attractor from time traces of the center of mass motion using lagged coordinates. Using only two lagged coordinates, scale-dependent Lyapunov exponents help distinguishing deterministic and noisy chaos from parameter regions where noise is dominant.[25] This is important because the phase transitions exist within the noisy chaos region. While scale-dependent Lyapunov exponents give qualitative information, we need six lagged coordinates to faithfully reconstruct the chaotic attractor and obtain the same LLEs as provided by the Benettin algorithm. This methodology will be important to ascertain whether a real system in nature exhibits scale-free-chaos phase transitions.

It is instructive to compare the scale-free-chaos phase transitions in the confined VM to the canonical paraferromagnetic equilibrium phase transition whose universality class comprises the Ising and ϕ^4 models. A phase is an

ergodic measure that exists in the thermodynamic limit (infinite volume and number of particles, finite density) and a phase transition corresponds to a discontinuous change from one to more than one phase as a parameter changes, i.e., to a bifurcation of the measure; see precise definitions and proofs in Ref. 38. Pure phases have different values of the magnetization order parameter. At the critical point that ends a line of first order phase transitions at zero external field, the correlation length becomes infinity in the thermodynamic limit[38]. The magnetization order parameter undergoes a pitchfork bifurcation at the critical temperature with critical exponent 0.327 instead of 0.5.[15,39]

The main objects to characterize critical points of second-order equilibrium phase transitions are static and dynamic correlation functions. To study flocking and other nonequilibrium phase transitions, we need to adapt the definitions of correlation functions, correlation length, susceptibility, and so on, to models such as Vicsek's. Averages over the number of particles, time averages and averages over realizations replace the ensemble averages of equilibrium statistical mechanics.[6] Since it is important that correlation functions reflect underlying dynamic attractors, velocity fluctuations are about center of mass velocities (which may be chaotic), without further subtraction of rotations or dilations which may modify dynamics.[11,12]

The chaotic phases in scale-free-chaos transitions are ergodic.[22,23] The transitions are second order: as $N \gg 1$, the order parameter is close to zero in the sparse single-cluster chaotic phase and the polarization is positive in the multicluster chaotic phase. To characterize scale free chaos, we have used the dynamic correlation function in Fourier space and its associated correlation-relaxation time.[13] For finite N, the maximum of the static correlation function in Fourier space occurs for some finite wavenumber which is proportional to reciprocal correlation length and produces the macroscopic correlation time. The latter becomes infinite (critical slowing down) as $N \to \infty$, which can be used to identify a phase transition. The correlation length proportional to $1/k_c$ (k_c is the wavenumber of the maximum zero-time correlation function) also becomes infinite. Importantly, when the correlation length is proportional to the system size, the system is scale free and finite size scaling detects phase transitions. Using the correlation time, finite-size scaling and numerical simulations, we have identified a line of single-to-multicluster chaos phase transitions in the region of noisy chaos of Fig. 3(a). We have ascertained the character of the transition by means of topological data analysis. The correlation length (measured as the maximum of the cumulative static correlation function) times k_c is approximately 2, close to observations of natural swarms.[13]. The numerically calculated critical exponents are compatible with those measured in natural midge swarms[13]. In particular, the dynamic critical exponent is $z = 1$, which is different from the larger dynamic exponents of other models. As confinement vanishes, the line of phase transitions collapses to zero, and so does the largest Lyapunov exponent, and therefore chaos disappears. This is consistent with Eq. (2) that bounds the product of correlation length and LLE by a finite speed of propagation. Further study involving the invariant measure of the chaotic attractors would be desirable to explore analogies with the phase ergodic measures of equilibrium thermodynamics.

Using the susceptibility of the real-space static correlation function and finite size scaling, we have found other lines $\beta_i(N;\eta)$ and $\beta_m(N;\eta)$ that go to zero at the same rate as $\beta_c(N;\eta)$ for $N \gg 1$ and have the same critical exponent ν. Ascertaining whether the lines $\beta_c(N;\eta)$, $\beta_i(N;\eta)$, and $\beta_m(N;\eta)$ describe ultimately the same phase transition requires hard mathematical analysis, not just numerical simulations. What can we say based on our numerical simulations? Firstly, lines $\beta_i(N;\eta)$, and $\beta_m(N;\eta)$ based on an inflection point and the corresponding local maximum of the susceptibility surely describe the same phase transition as $N \to \infty$. This is also backed by our numerical simulations that produce the same critical exponent γ, for $\beta_i(N;\eta)$ and $\beta_m(N;\eta)$, notwithstanding their different dynamical critical exponents $z_i = 1.5$ and $z_m = 2$ (needed for NDCCF collapse), respectively. This difference may simply point to the multiple time scales involved in this phase transition. Secondly, the three critical lines tend to zero at the same rate as $N \to \infty$ because their exponent ν is the same but the exponent γ of $\beta_c(N;\eta)$ is different within the scope of our numerical simulations ($N \leq 5000$). There are two possibilities. One. There are two different lines of phase transitions represented by $\beta_c(N;\eta)$ and either $\beta_i(N;\eta)$ or $\beta_m(N;\eta)$. Then scale-free chaos and power laws extend beyond $\beta_c(N;\eta)$, albeit to lines in a region that vanishes as $N \to \infty$ and all β tend to 0. Two. There is a single phase transition of scale free chaos for each η. The different values of the static critical exponent γ reflect how the different length scales involved in the multifractal chaotic attractor, cf Fig. 7(b), affect the susceptibility, whereas the different values of the dynamic critical exponent z reflect the different time scales involved in the chaotic attractor. The correlation lengths, as calculated from either the real space or Fourier transform of the static correlation function, produce the same exponent ν for all β lines.

At this point, we *conjecture* that there is a sole phase transition for each admissible noise value. Then, the only line consistent with all relations defining critical exponents, Eqs. (5)-(8), is $\beta_c(N;\eta)$ (single to multicluster chaos). The set of critical exponents for the lines $\beta_c(N;\eta)$ is compatible with those observed in natural midge swarms. The static critical exponent $\nu = 0.44 \pm 0.02$ is close to measured $\nu = 0.35 \pm 0.10$ (within error estimates). The exponent γ should be calculated from the line $\beta_m(N;\eta)$ to compare with measurements of natural swarms. However unlike in our simulations, measurements involved elimination of rotations and dilation from the center-of-mass velocity.[11,12] This may explain why the exponent $\gamma_m = 1.15$ is different from the measured $\gamma = 0.9$. If we define the average velocity of the swarm taking into account rotations and dilations, the local maxima of the susceptibility versus confinement shift considerably to the end of the first chaotic window in Fig. 8(b) and no longer correspond to the scale-free-chaos transition considered here. The dynamic exponent $z = 1$ calculated from the simulations produces collapse of the NDCCF and is compatible with measured NDCCF collapse from swarm data; see Fig. SF2 in Ref. 13. Un-

like equilibrium phase transitions for which the NDCCF collapses into a single curve as a function of $k^z t$, NDCCF collapse at $\beta_c(N;\eta)$ occurs only for smaller times, $0 < kt < 4$, cf Fig. 5(b). That the NDCCF collapses only at short times for $0 < kt < 4$ is also observed in natural swarms.[13]

Several time scales are involved in codimension two (and higher) bifurcations of dynamical systems;[40] see e.g., the scaled normal form in Ref. 41. The mean field version of the standard two-dimensional Vicsek model with periodic boundary conditions also involves two time scales near the order-disorder transition. The mean field VM can be described by a discrete-time Enskog-type kinetic equation which preserves the overall number of particles[42]. The order-disorder phase transition appears as a supercritical bifurcation of the kinetic equation when one multiplier crosses the unit circle in the complex plane; another multiplier corresponding to particle conservation is always one[43]. On the ordered side, the scaled bifurcation equations contain two time scales, one with $z = 1$ (hyperbolic scaling), the other with $z = 2$ (parabolic scaling). At the hyperbolic short time scale, undamped wave propagation and resonance phenomena arise[43], whereas different patterns appear at the parabolic time scale further from the bifurcation point[44]. These patterns exist on the ordered side of the ordering phase transition. They can be found in direct simulations of the standard Vicsek model and include bands[45] and crossbands[46].

A universality class comprises all physical systems that evolve to the same fixed point of the renormalization group equations under a rescaling of space and time and therefore have the same critical exponents[7]. Even if the renormalization group equations are not known, systems with the same critical exponents belong to the same universality class. Arguably, natural swarms belong to a novel dynamic universality class with dynamic critical exponent $z \approx 1$ independent of $k\xi$ and flat NDCCF at small times[13]. Curiously, $z = 1$ corresponds to the hyperbolic time scale of the order-disorder transition in the VM with periodic boundary conditions.[43] At the scale-free-chaos phase transitions between single and multicluster chaos, the confined VM satisfies these requirements. At moderate N, this transition is different from the well-known period-doubling, intermittency and quasiperiodic routes to chaos[22,23,28]. It encompasses phenomena at different time scales, from dynamical exponent $z = 1$ to larger z for β_i and β_m, which might require theoretical tools sharper than correlation functions to understand. Would it be possible to derive effective equations near the scale-free-chaos phase transition playing roles similar to amplitude equations in bifurcation theory?[47] Time will tell.

Summarizing, we have numerically simulated the harmonically confined Vicsek model, which is an idealized description of insect swarms. Depending on confinement strength β and noise η, the model exhibits different periodic, quasiperiodic and chaotic attractors. Our results support the existence of a line of phase transitions in a noisy chaos region of η values as the number of particles N tends to infinity and $\beta \to 0$. For finite N, there is a line $\beta_c(N;\eta)$ at which the correlation time is minimal and the correlation length is proportional to the system size. Topological data analysis supports the interpretation of $\beta_c(N;\eta)$ as a line separating single from multicluster chaos. The time averaged polarization acts as an order parameter: near $\beta_c(N;\eta)$, it is almost zero for $\beta < \beta_c(N;\eta)$ and positive and increasing with β for $\beta > \beta_c(N;\eta)$. On the line of scale free chaos, the dynamic critical exponent is $z = 1$ and the dynamic correlation function collapses on an interval of the same length as in measured swarms. Other possible descriptions of the transitions involve the maximum of the susceptibility at fixed N and η, which produce lines $\beta_i(N;\eta)$ and $\beta_m(N;\eta)$. These lines have the same critical exponent ν for the correlation length as $\beta_c(N;\eta)$, which supports our conjecture that all three lines represent the same scale-free-chaos phase transitions. Different exponents z and γ on the lines may reflect the multiplicity of time and length scales involved in the chaotic attractors. Compared to measurements in natural swarms, $z = 1$ and $\nu = 0.44$ are quite similar to measured exponents and γ is larger.

This work paves the way to studies in many directions. Many directions consist of exploring other possible transitions on chaotic and non-chaotic windows of the parameter space. On the theoretical side, can we find the invariant measure of the chaotic attractors and characterize scale-free-chaos phase transitions as $N \to \infty$ in terms of the invariant measure? This could bring together dynamical systems and nonequilibrium statistical mechanics studies and yield fruitful new ideas and methods.

ACKNOWLEDGMENTS

This work has been supported by the FEDER/Ministerio de Ciencia, Innovación y Universidades – Agencia Estatal de Investigación grantsPID2020-112796RB-C21 (RGA & AC) and PID2020-112796RB-C22 (LLB), by the Madrid Government (Comunidad de Madrid-Spain) under the Multiannual Agreement with UC3M in the line of Excellence of University Professors (EPUC3M23), and in the context of the V PRICIT (Regional Programme of Research and Technological Innovation) (LLB). RGA acknowledges support from the Ministerio de Economía y Competitividad of Spain through the Formación de Doctores program cofinanced by the European Social Fund.

DATA AVAILABILITY STATEMENT

Data available on request from the authors

Appendix A: Nondimensionalized equations of the confined Vicsek model

We consider the three-dimensional confined Vicsek model:

$$\mathbf{x}_j(t+\Delta t) = \mathbf{x}_j(t) + \Delta t\, \mathbf{v}_j(t+\Delta t),$$
$$\mathbf{v}_i(t+\Delta t) = v\mathscr{R}_\eta \left[\frac{\sum_{|\mathbf{x}_j-\mathbf{x}_i|<r_1 R_0} \mathbf{v}_j(t) - \beta_0 \mathbf{x}_i(t)}{\left| \sum_{|\mathbf{x}_j-\mathbf{x}_i|<r_1 R_0} \mathbf{v}_j(t) - \beta_0 \mathbf{x}_i(t) \right|} \right], \quad \text{(A1)}$$

where $\mathscr{R}_\eta(\mathbf{w})$ rotates the unit vector $\mathbf{w}$ randomly within a spherical cone centred at it and spanning a solid angle in $(-\frac{\eta}{2},\frac{\eta}{2})$. Initially, the particles are randomly placed within a sphere with unit radius and the particle velocities are pointing outwards.

We nondimensionalize the model using data from the experiments on midges reported in the supplementary material of Refs. 11–13. We select the event labeled 20120910_A1 in Table I[13]. We measure times in units of $\Delta t = 0.24$ s, lengths in units of the time-averaged nearest-neighbor distance of the 20120910_A1 swarm, which is $r_1 = 4.68$ cm, and velocities in units of $r_1/\Delta t$, whereas $v = 0.195$ m/s. Then Eq. (1) is the nondimensional version of Eq. (A1) with $\Delta t = 1$ and

$$v_0 = v\frac{\Delta t}{r_1}, \quad \beta = \beta_0 \Delta t. \tag{A2}$$

For the example we have selected, $v_0 = 1$, whereas other entries in the same table produce order-one values of v_0 with average 0.53. For these values, the confined Vicsek model has the same behavior as described here. Thus, the Vicsek model describing midge swarms is far from the continuum limit $v_0 \ll 1$. Cavagna *et al* consider a much smaller speed, $v_0 = 0.05$, closer to the continuum limit where derivatives replace finite differences[13].

Collective consensus is quantified by the polarization $W \in [0,1]$:

$$W(t;\eta,\beta) = \left| \frac{1}{N}\sum_{j=1}^{N} \frac{\mathbf{v}_j(t)}{|\mathbf{v}_j(t)|} \right|. \tag{A3}$$

The time average $\langle W\rangle_t$ coincides with the ensemble average of (A3) by ergodicity.

Effect of the boundary conditions. In the standard VM, the particles are enclosed in a cubic box, the boundary conditions are periodic and the system is invariant under translations. On the other hand, in the confined VM, there are no boundaries, the particles are confined by a harmonic potential, and translation invariance is broken. There are many studies of the standard VM, which is not the case for the confined VM. In fact, the confined VM has time-dependent attractors that are different from those of the standard VM. Among them, chaotic attractors. Another qualitative difference between both VMs is that broken translation symmetry precludes particles filling uniformly the available space for the confined VM. Thus, the ordering transition of the periodic-box VM cannot be the same for the confined VM.

Appendix B: Chaotic and noisy dynamics

We calculate the LLE in different ways that are complementary to each other: (i) directly from the equations by using the Benettin *et al* (BA) algorithm[21–23], (ii)-(iii) using from time traces of the center-of-mass motion or the NDCCF to reconstruct the phase space of the chaotic attractor. We need model equations to use the BA whereas time traces can be obtained from numerical simulations of equations or from experiments and observations. To obtain the LLE from time traces, we have used (ii) the scale-dependent Lyapunov exponent (SDLE) algorithm[25] and (iii) the Gao-Zheng algorithm[24]. The SDLE algorithm is useful to separate the cases of mostly deterministic chaos from noisy chaos and mostly noise even in the presence of scarce data and a reconstruction of the attractor that is not very precise[25] whereas the Gao-Zheng algorithm requires more data points[24]. We now describe these different algorithms and illustrate the results they provide for the confined VM. In all cases, we eliminate the effects of initial conditions by leaving out the first 30000 time steps before processing the time traces.

1. Benettin algorithm

We have to simultaneously solve Eqs. (1) and the linearized equations

$$\delta\tilde{\mathbf{x}}_i(t+1) = \delta\tilde{\mathbf{x}}_i(t) + \delta\tilde{\mathbf{v}}_i(t+1), \quad i = 1,\dots,N, \tag{B1a}$$

$$\delta\tilde{\mathbf{v}}_i(t+1) = v_0 \mathscr{R}_\eta \left[\left(\mathbb{I}_3 - \frac{[\sum_{|\mathbf{x}_j-\mathbf{x}_i|<R_0} \mathbf{v}_j(t) - \beta\mathbf{x}_i(t)]^T [\sum_{|\mathbf{x}_j-\mathbf{x}_i|<R_0} \mathbf{v}_j(t) - \beta\mathbf{x}_i(t)]}{|\sum_{|\mathbf{x}_j-\mathbf{x}_i|<R_0} \mathbf{v}_j(t) - \beta\mathbf{x}_i(t)|^2} \right) \cdot \frac{\sum_{|\mathbf{x}_j-\mathbf{x}_i|<R_0} \delta\tilde{\mathbf{v}}_j(t) - \beta\delta\tilde{\mathbf{x}}_i(t)}{|\sum_{|\mathbf{x}_j-\mathbf{x}_i|<R_0} \mathbf{v}_j(t) - \beta\mathbf{x}_i(t)|} \right], \tag{B1b}$$

in such a way that the random realizations $\mathscr{R}_\eta$ are exactly the same for Eqs. (1) and (B1). The initial conditions for the disturbances, $\delta\tilde{\mathbf{x}}_i(0)$ and $\delta\tilde{\mathbf{v}}_i(0)$, can be randomly selected so that the overall length of the vector $\delta\boldsymbol{\chi} = (\delta\tilde{\mathbf{x}}_1,\dots,\delta\tilde{\mathbf{x}}_N,\delta\tilde{\mathbf{v}}_1,\dots,\delta\tilde{\mathbf{v}}_N)$ equals 1. After each time step t, the vector $\delta\boldsymbol{\chi}(t)$ has length α_t. At that time, we renormalize $\delta\boldsymbol{\chi}(t)$ to $\hat{\chi}(t) = \delta\boldsymbol{\chi}(t)/\alpha_t$ and use this value as initial condition to calculate $\delta\boldsymbol{\chi}(t+1)$. With all the values α_t and for sufficiently large l, we calculate the Lyapunov exponent as

$$\lambda_1 = \frac{1}{l}\sum_{t=1}^{l} \ln\alpha_t, \tag{B2}$$

$$\alpha_t = |\delta\boldsymbol{\chi}(t)| = |(\delta\tilde{\mathbf{x}}_1(t),\dots,\delta\tilde{\mathbf{x}}_N(t),\delta\tilde{\mathbf{v}}_1(t),\dots,\delta\tilde{\mathbf{v}}_N(t))|,$$

Fig. 15 plots λ_1 versus l at critical confinement $\beta = \beta_c(N)$ showing convergence of the exponent for different values of N. For $N = 750$, Fig. 16(a) depicts the LLE versus l for different values of β whereas Fig. 16(c) fixes $\beta = \beta_c(750) = 0.0035$

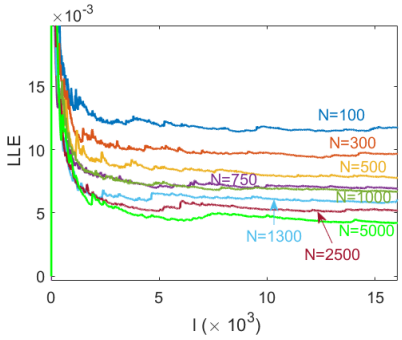

FIG. 15: Largest Lyapunov exponent as a function of l as given by Eq. (B2) for $\eta = 0.5$, $\beta = \beta_c(N)$ and different N

and shows the LLE versus l for different values of N, including $N = 750$. These figures indicate that the LLE is not a monotonic function of either β or N. Figs. 16(c) (green point) and 16(d) (purple point) show that the points corresponding to critical confinement are located on the increasing branches of the LLE versus β and N.

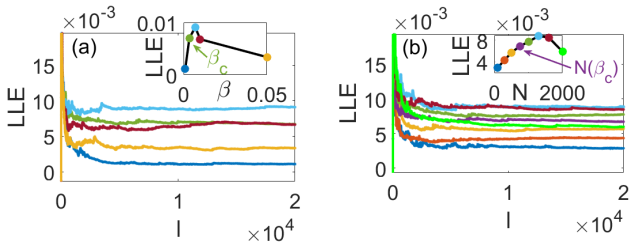

FIG. 16: **(a)** LLE versus l as in Eq. (B2) for $N = 750$ and $\beta = 0.001, 0.0035, 0.007, 0.01, 0.05$. Inset: LLE vs β; marked: $\beta_c = 0.0035$. **(b)** LLE vs l for $\beta = 0.0035$ and $N = 100, 300, 500, 750, 1000, 1300, 1600, 2000$. Inset: LLE vs N for $\beta_c = 0.0035$; marked: $N = 750$. Here $\eta = 0.5$.

2. Scale dependent Lyapunov exponents

We use scale dependent Lyapunov exponents (SDLE) from the CM motion to characterize deterministic and noisy chaos as different from noise[25].

Adding the components of $\mathbf{X}(t)$, we form the time series $x(t) = X_1(t) + X_2(t) + X_3(t)$. To calculate the SDLE, we construct the lagged vectors: $\mathbf{X}_i = [x(i), x(i+\tilde{\tau}), .., x(i+(m-1)\tilde{\tau})]$. The simplest choice is $m = 2$ and $\tilde{\tau} = 1$ (other values can be used, see below). From this dataset, we determine the maximum $\varepsilon_{\max}$ and the minimum $\varepsilon_{\min}$ of the distances between two vectors, $\|\mathbf{X}_i - \mathbf{X}_j\|$. Our data is confined in $[\varepsilon_{\min}, \varepsilon_{\max}]$. Let ε_0, ε_t and $\varepsilon_{t+\Delta t}$ be the average separation between nearby trajectories at times 0, t, and $t + \Delta t$, respectively. The SDLE is

$$\ln \lambda(\varepsilon_t) = \frac{\ln \varepsilon_{t+\Delta t} - \ln \varepsilon_t}{\Delta t}. \tag{B3a}$$

The smallest possible Δt is of course the time step $\tilde{\tau} = 1$, but Δt may also be chosen as an integer larger than 1. Gao *et al* introduced the following scheme to compute the SDLE[25]. Find all the pairs of vectors in the phase space whose distances are initially within a shell of radius ε_k and width $\Delta\varepsilon_k$:

$$\varepsilon_k \le \|\mathbf{X}_i - \mathbf{X}_j\| \le \varepsilon_k + \Delta\varepsilon_k, \quad k = 1, 2, \ldots. \tag{B3b}$$

We calculate the Lyapunov exponent as follows:

$$\lambda(\varepsilon_t) = \frac{\langle \ln \|X_{i+t+\triangle t} - X_{j+t+\triangle t}\| - \ln \|X_{i+t} - X_{j+t}\| \rangle_k}{\triangle t}, \tag{B3c}$$

where $\langle\rangle_k$ is the average within the shell $(\varepsilon_k, \varepsilon_k + \triangle\varepsilon_k)$. The shell dependent SDLE $\lambda(\varepsilon)$ in Fig. 3(b) displays the dynamics at different scales for $\tilde{\tau} = 1$ and $m = 2$.[25] Using 2 lagged coordinates produces plateaus having a value of $\lambda(\varepsilon)$ equal to the LLE of deterministic chaos. This value differs from the LLE calculated using the BA or a more appropriate reconstruction of the phase space involving more lagged coordinates (see below). However, the SDLE with $m = 2$ yields a qualitative idea of the effects of noise on chaos. In deterministic chaos, $\lambda(\varepsilon) > 0$ presents a plateau with ends $\varepsilon_1 < \varepsilon_2 \ll 1$, in noisy chaos, this plateau is preceded and succeeded by regions in which $\lambda(\varepsilon)$ decays as $-\gamma \ln \varepsilon$, whereas it shrinks and disappears when noise swamps chaos. As η increases, $\lambda(\varepsilon)$ first decays to a plateau for $\eta = 0.1$. A criterion to distinguish (deterministic or noisy) chaos from noise is to accept the largest Lyapunov exponent as the positive value at a plateau $(\varepsilon_1, \varepsilon_2)$ satisfying

$$\log_{10} \frac{\varepsilon_2}{\varepsilon_1} \ge \frac{1}{2}. \tag{B3d}$$

For $\eta = 0.5$, the region where $\log_{10}(\varepsilon_2/\varepsilon_1) = 1/2$ is marked in Fig. 3(b) by vertical lines. Plateaus with smaller values of $\log_{10}(\varepsilon_2/\varepsilon_1)$ or their absence indicate noisy dynamics[25]. This occurs for $\eta = 1$. The ends of the interval $(0.1, 1)$ of noisy chaos are marked by two vertical dashed lines in Fig. 3(a).

The chaotic dynamics of the swarm is reflected in quantities that depend on the positions and velocities of the particles. Important global quantities are the motion of the CM and the NDCCF of Eq. (3). Figs. 17 displays the CM trajectory, thereby visualizing the dynamics of the swarm. For increasing values of noise corresponding to the different regions in Fig 3(a), the CM motion goes from deterministic chaos, Fig. 17(a), to noisy chaos, Fig. 17(b), to mostly noise, Fig. 17(c).

Note that all the plateaus in Fig. 3(b) produce the same pos-

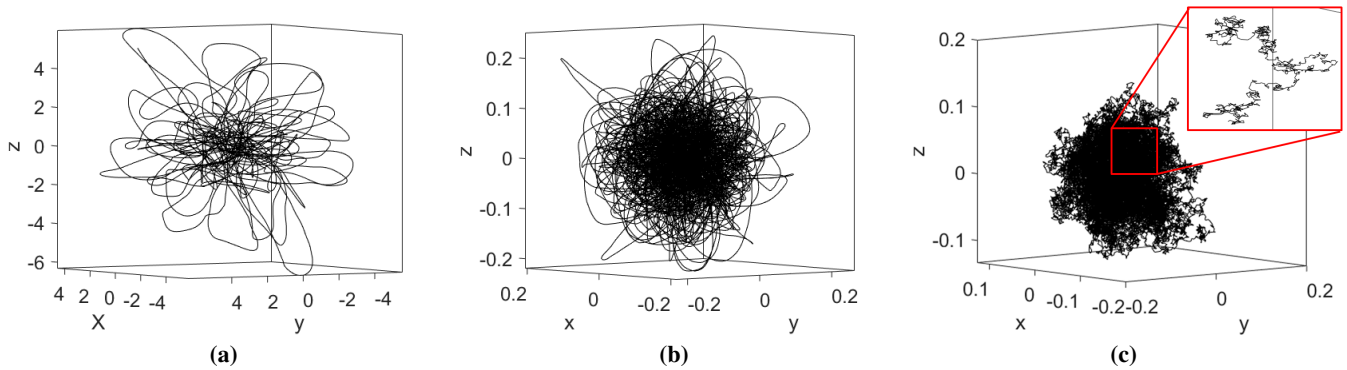

(a) **(b)** **(c)**

FIG. 17: **(a)** Trajectory of the center of mass for $\eta = 0.01$, which corresponds to deterministic chaos with flower shape phase portrait. **(b)** Same for $\eta = 0.3$, which corresponds to noisy chaos: the trajectories of the center of mass cover more densely part of the space. **(c)** Predominantly noisy motion for $\eta = 5.5$. The trajectories from $t_0 = 1000$ to $t_f = 50000$ are depicted. Here, $N = 100$, $\beta = \beta_c$ for each η, and the unit of length is 1 meter.

itive value of the LLE $\lambda(\varepsilon)$. This is not very realistic because the BA yields different values of the LLE depending on the noise strength η. Why? Recall that we have used $m = 2$ (two lagged coordinates) in the reconstruction of the attractor from the time traces. However, as shown in Fig. 7(b), the CM chaotic attractor has fractal dimension D_0 between 2 and 3, and we need $m \geq 2D_0$ to faithfully reconstruct the chaotic attractor[22,23]. Thus, we need at least $m = 6$ to reconstruct it. Using $m = 6$ and its optimal value of $\tilde{\tau}$ (Ref. 24) produces Fig. 3(c). Now $\lambda(\varepsilon)$ presents large oscillations whose averages in the plateau regions coincide with the LLE as calculated by the Gao-Zheng algorithm[24].

3. Largest Lyapunov exponent from high dimensional reconstructions of CM motion

As explained above, the previous reconstruction of the phase space for CM motion used to calculate SDLE considers 2D lagged vectors ($m = 2$). This produces useful qualitative phase diagrams with flat plateaus, but the dimension of this vector space is too small to reconstruct faithfully the attractor. More realistic CM trajectories in higher dimension contain self-intersections in dimension 2. This explains the different values of the LLE found in the SDLE plateaus of Fig. 3(b) as compared with those found by the BA of Eq. (B2). To reconstruct safely a chaotic attractor, the dimension of the lagged vectors should surpass twice the fractal dimension D_0.[22] For the confined VM, $m = 6$ is sufficient in view of Fig. 7(b). However, the SDLE $\lambda(\varepsilon)$ presents oscillations as indicated in Fig. 3(c) and their average values replace the plateaus in Fig. 3(b). In contrast with Fig. 3(b), the averaged oscillations produce LLEs that increase with noise. Averaging oscillations is not going to produce precise values of the LLE. Thus, we calculate the LLE from the lagged coordinates with $m = 6$ using the Gao-Zheng algorithm[24]. This requires constructing the quantity $\Lambda(k)$ whose slope near the origin gives the LLE[24]

$$\Lambda(k) = \left\langle \ln \frac{\|X_{i+k} - X_{j+k}\|}{\|X_i - X_j\|} \right\rangle. \qquad \text{(B4)}$$

Here the brackets indicate ensemble average over all vector pairs with $\|X_i - X_j\| < r^*$ for an appropriately selected small distance r^*. Fig. 18 displays the graph of $\Lambda(k)$ given by Eq. B4. The slopes of $\Lambda(k)$ for different values of N at $\beta_c(N)$ equal the LLEs, increase with β and agree with the averaged oscillations marked in Fig. 3(c).

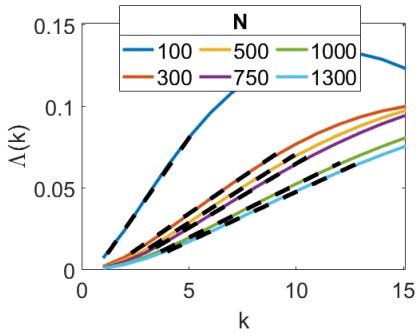

FIG. 18: Plot of $\Lambda(k)$ vs k for different values of β. Thick dashed lines mark the slope of $\Lambda(k)$ for different values of N at $\beta_c(N)$.

N	100	300	500	750	1000	1300
BA	0.0118	0.0095	0.0078	0.0070	0.0067	0.0058
CM	0.017	0.0092	0.008	0.007	0.0063	0.0059
g(t)	0.0055	0.0044	0.0041	0.0038	0.0035	0.0033

TABLE I: LLE for $\eta = 0.5$ and different N at $\beta_c(N;\eta)$ as calculated using the BA for the complete VM equations, Eq. (B2), and Eq. (B4) for CM motion and for the NDCCF $g(t)$. Note that the LLE as calculated using the BA and Eq. (B4) for CM motion are similar whereas the LLE corresponding to the NDCCF $g(t)$ is smaller.

For different particle numbers with $\eta = 0.5$, Table I lists the LLEs calculated using the BA for the complete system as in

Eq. (B2), and using Eq. (B4) for CM motion and for the NDCCF $g(t)$. We observe that the LLE values calculated from the CM motion are similar to those found by the BA, whereas they are noticeably smaller if calculated for the NDCCF. While the NDCCF is still chaotic, we speculate that the subtraction of the CM motion and ensemble average involved in two-time NDCCF $g(t)$ dilute chaos by lowering the LLE.

Appendix C: Dynamic and static connected correlation functions

Following Refs. 11 and 12, we define the dynamic connected correlation function (DCCF) as

$$C(r,t)=\left\langle \frac{\sum_{i=1}^{N}\sum_{j=1,j\neq i}^{N}\delta\hat{\mathbf{v}}_i(t_0)\cdot\delta\hat{\mathbf{v}}_j(t_0+t)\delta[r-r_{ij}(t_0,t)]}{\sum_{i=1}^{N}\sum_{j=1,j\neq i}^{N}\delta[r-r_{ij}(t_0,t)]}\right\rangle_{t_0} \quad \text{(C1)}$$

$$C(r)=C(r,0),$$

$$\delta\hat{\mathbf{v}}_i=\frac{\delta\mathbf{v}_i}{\sqrt{\frac{1}{N}\sum_k\delta\mathbf{v}_k\cdot\delta\mathbf{v}_k}},\quad \delta\mathbf{v}_i=\mathbf{v}_i-\mathbf{V},$$

$$r_{ij}(t_0,t)=|\mathbf{r}_i(t_0)-\mathbf{r}_j(t_0+t)|,\ \mathbf{r}_i(t_0)=\mathbf{x}_i(t_0)-\frac{1}{N}\sum_{j=1}^{N}\mathbf{x}_j(t),$$

$$\langle f\rangle_{t_0}=\frac{1}{t_{max}-t}\sum_{t_0=1}^{t_{max}-t}f(t_0,t).$$

In these equations, $\delta(r-r_{ij})=1$ if $r<r_{ij}<r+dr$ and zero otherwise, and dr is the space binning factor. The usual dynamic correlation function and susceptibility in statistical mechanics are

$$C(r,t)=\langle(\phi(0,0)-\langle\phi(0,0)\rangle)(\phi(\mathbf{r},t)-\langle\phi(\mathbf{r},t)\rangle)\rangle, \quad \text{(C2a)}$$

$$\chi=\int C(r,0)\,d\mathbf{r}=\hat{C}(0,0), \quad \text{(C2b)}$$

respectively, where $\langle\ldots\rangle$ are averages over the appropriate ensemble average. In Eq. (C1), we have have replaced arithmetic means instead of the ensemble averages and added a time average. Dropping the condition $j\neq i$ adds one term proportional to $\delta(r)$ to numerator and denominator of Eq. (C1), which is the choice made in Refs. 6 and 13.

The function $C(r,t)$ sums all the products $\delta\mathbf{v}_i(t_0)\cdot\delta\mathbf{v}_j(t_0+t)$ for those pairs i andj with a distance $r_{ij}(t_0,t)$ between r and $r+dr$, and then divides by the number of such pairs (denominator). It depends only on the distance r at time t because inter-particle interactions are local and distance dependent. The static connected correlation function (SCCF) is the equal time connected correlation function given by Eq. (C1). As discussed in Refs. 6 and 13, these definitions are inspired in statistical mechanics taking into account $\sum_j\delta\hat{\mathbf{v}}_j=0$ because ensemble averages have been replaced by averages over the particles.

For a SCCF that decays exponentially, the correlation length ξ is such that $C(\xi)=1/e$. In the present work, there is finite size scaling[11–13] and $C(r)$ or $C(r,t)$ do not decay exponentially with r and can take on negative values. Then the correlation length ξ is the first zero of $C(r)$, corresponding to the first maximum of the cumulative correlation function:[11,12]

$$Q(r)=\frac{1}{N}\sum_{i=1}^{N}\sum_{j\neq i}^{N}\delta\hat{\mathbf{v}}_i\cdot\delta\hat{\mathbf{v}}_j\theta(r-r_{ij}),\quad \chi=Q(\xi), \quad \text{(C3)}$$

$$\xi=\text{argmax}Q(r),\ C(\xi)=0 \text{ with } C(r)>0,\ r\in(0,\xi),$$

where $\theta(x)$ is the Heaviside unit step function. It turns out that this correlation length ξ is proportional to the swarm size ℓ, which is the hallmark of scale free behavior. At equilibrium, the susceptibility measures the response of the order parameter to changes in an external field linearly coupled to it, and equals the integral of the SCCF (C2b) with $C(r)>0$. A susceptibility thus defined would be $Q(\infty)$. However, by Eq. (C3), $Q(\infty)=Q(\ell)=-1$ because $\theta(\ell-r_{ij})=1$ and $\sum_i\delta\hat{\mathbf{v}}_i=0$. Thus, we cannot define susceptibility by Eq. (C2b). Instead, we define susceptibility χ as the value of $Q(r)$ at its first maximum, as in Eq. (6), and Refs. 11 and 12. For values of N corresponding to insects in measured swarms, our numerical simulations produce susceptibility values defined by Eq. (C3) between 0.7 and 1.2, which are included in the measured interval $(0.32,5.57)$.[11,12]

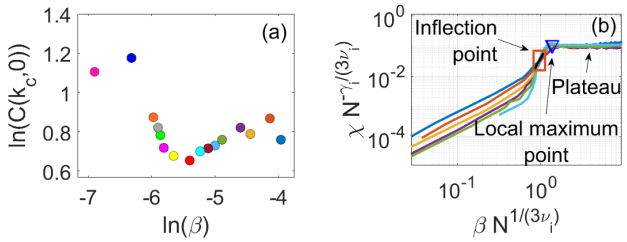

FIG. 19: **(a)** Log-log scale plot of the susceptibility as given by $\max_k\hat{C}(k,0)$ of Eq. (3) versus β_c. **(b)** Scaled susceptibility versus scaled confinement showing data collapse at the inflection point (square) and the local maximum (triangle) of the susceptibility. The local maximum is followed by a plateau of the scaled confinement. Here $\eta=0.5$, $\nu_i=0.44$, $\gamma_i=1.2$.

At equilibrium and for $N=\infty$, the susceptibility becomes infinity at critical points and it marks a phase transition. The susceptibility scales as

$$\chi(x)\sim(x-x_c)^{-\gamma}, \quad \text{(C4)}$$

where x is the control parameter and x_c the value thereof for $N=\infty$. In our case, $x=\beta_c(N,\eta)$ and $x_c=\beta_c(\infty,\eta)=0$, which produces $\gamma=0.92\pm0.05$ as shown in Fig. 6(b). Eq. (3) is related to the Fourier transform of $C(r,t)$, as discussed in Ref. 6. Fig. 19(a) shows that $\hat{C}(k,0)$ of Eq. (3) oscillates with $\beta_c(N;\eta)$. Thus, $\max_k\hat{C}(k,0)$ is not a convenient definition of susceptibility. Contrastingly, Fig. 6(b) plots the real-space susceptibility $\max_r Q(r)$ using many more values, $500\leq N\leq 5000$, which makes this fitting more reliable and similar to the measured values in Refs. 11 and 12. Fig. 19(b)

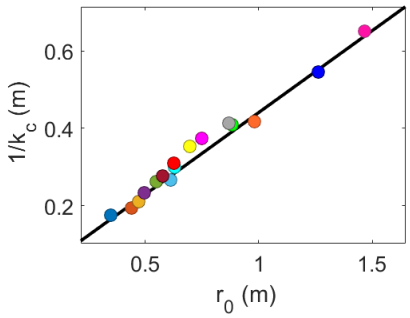

FIG. 20: The correlation length $\xi = 1/k_c$ computed from the static correlation function in Fourier space as a function of the correlation length $\xi = r_0$ computed from the static correlation function in real space. Unit of length is 1 meter.

shows data collapse of scaled susceptibility and scaled confinement at β_i (susceptibility inflection point) and β_m (susceptibility local maximum). For our data, the relation between the correlation length as defined by Eq. (C3) and $1/k_c$, given by $k_c = \text{argmax}_k \hat{C}(k,0)$ is

$$\frac{1}{k_c} = 0.440\, r_0 + 0.017, \tag{C5}$$

where $1/k_c$ and r_0 are measured in meters; see Fig. 20. Note that the straight line in Fig. 20 is quite close to that of Fig. SF1 of Ref. 13 (Supplementary data) obtained from measurements in natural midge swarms.

Instead of setting $x = \beta$, we can use the rescaled average nearest neighbor distance $x = r_1/R_0$ (perception range, inversely proportional to density), as in Ref. 11 and 12. We find a critical perception range $x_c = 2.945 \pm 0.047$ ($x - x_c \sim \beta$). This is larger than $x_c = 0.421 \pm 0.002$ at the order-disorder transition of the standard VM[11,12], indicating a less dense swarm at critical confinement. As $x_c = 12.5 \pm 0.1$ in natural swarms (measured in units of the average insect size)[11,12], the critical perception range is 4.2 insect bodies for the scale-free chaotic transition of the confined Vicsek model versus 30 insect sizes at the order-disorder transition.

As chaos disappears when $\beta \to 0$, it may seem surprising that an ordered chaotic phase is less dense than the disordered phase at the larger noise of the order-disorder transition for the standard VM with periodic boundary conditions. Recall that density is inversely proportional to the average nearest neighbor distance (perception range). However, the confined VM does not morph seamlessly to the standard VM as $\beta_c(N;\eta) \to 0$. Firstly, confinement by a harmonic potential and confinement due to a large box with periodic boundary conditions are qualitatively different and that they may not produce the same swarm patterns in the thermodynamic limit. Secondly, the standard VM with periodic boundary conditions experiences a crossover to a discontinuous order-disorder phase transition for $N \gg 1$.[20] We do not know whether the confined VM experiences such a crossover for the parameter range of interest. Thirdly, the noise values for which the confined VM and the standard VM with periodic boundary conditions have similar critical behaviors[13] are much larger than the noisy chaos interval of Fig. 3(a). Thus, we think that the scale-free-chaos phase transition of the confined VM as $\beta \to 0$ is not related to the continuous order-disorder transition of the standard VM.

In Refs. 11 and 12, the average swarm velocity is defined subtracting overall rotations and dilations from $\mathbf{V}$ at each time step. These subtractions affect considerably the dynamics of the system. We have observed that the local maxima of the susceptibility versus confinement shift considerably to the end of the first chaotic window in Fig. 8(b). They no longer correspond to the scale-free-chaos transition considered here. The inflection points of the susceptibility versus confinement are more robust. We have calculated the critical exponents ν and γ using these points. The exponent ν remains the same but γ is now smaller, $\gamma_i = 0.70 \pm 0.06$ (calculated for $N \leq 2000$).

To calculate the connected correlation functions, we proceed as follows. Fixing the parameters N, η and β, we simulate the VM for five different random initial conditions during 10000 iterations. After a sufficiently long transient period, the polarization of Eq. (A3) fluctuates about a constant value. Once this regime is established, we use the last 2000 iterations to calculate the static correlation function $\hat{C}(k,0)$, whose first maximum provides the critical wave number k_c. Using the definition in Eq. (3) and averaging over the five realizations, we obtain the time dependent correlation function.

[1] T. Mora, W. Bialek, Are Biological Systems Poised at Criticality? J. Stat. Phys. **144**, 268-302 (2011).
[2] W. S. Bialek, Biophysics: Searching for Principles (Princeton University Press, Princeton, 2012).
[3] Q.-Y. Tang, Y. Y. Zhang, Y. Wang, W. Wang, D. R. Chialvo, Critical fluctuations in the native state of proteins. Phys. Rev. Lett. **118**, 088102 (2017).
[4] D. J. T. Sumpter, *Collective Animal Behavior* (Princeton University Press, 2010).
[5] M. Azaïs, S. Blanco, R. Bon, R. Fournier, M.-H. Pillot, J. Gautrais, Traveling pulse emerges from coupled intermittent walks: A case study in sheep. PLoS ONE **13**(12), e0206817 (2018).
[6] A. Cavagna, I. Giardina, T.S. Grigera, The physics of flocking: Correlation as a compass from experiments to theory. Phys. Rep. **728**, 1-62 (2018).
[7] K. Huang, *Statistical Mechanics. 2nd ed* (Wiley, NY, 1987).
[8] A. Okubo, Dynamical aspects of animal grouping: Swarms, schools, flocks, and herds. Adv. Biophys. **22**, 1-94 (1986).
[9] A. Okubo, S. A. Levin, *Diffusion and Ecological Problems: Modern Perspectives, 2nd ed* (Springer, NY, 2001).
[10] J. G. Puckett, N. T. Ouellette, Determining asymptotically large population sizes in insect swarms. J. Roy. Soc. Interface **11**, 20140710 (2014).
[11] A. Attanasi, A. Cavagna, L. Del Castello, I. Giardina, S. Melillo, L. Parisi, O. Pohl, B. Rossaro, E. Shen, E. Silvestri, M. Viale, Collective Behaviour without Collective Order in Wild Swarms of Midges. PLoS Comput. Biol. **10**(7), e1003697 (2014).
[12] A. Attanasi, A. Cavagna, L. Del Castello, I. Giardina, S. Melillo, L. Parisi, O. Pohl, B. Rossaro, E. Shen, E. Silvestri, M. Viale, Finite-Size Scaling as a Way to Probe Near-Criticality in Natural Swarms. Phys. Rev. Lett. **113**, 238102 (2014).
[13] A. Cavagna, D. Conti, C. Creato, L. Del Castello, I. Giardina, T. S. Grigera, S. Melillo, L. Parisi, M. Viale, Dynamic scaling in natural swarms. Nat. Phys. **13**(9), 914-918 (2017).
[14] B. I. Halperin, P. C. Hohenberg, Scaling laws for dynamic critical phenomena. Phys. Rev. **177**, 952-971 (1969).
[15] D. J. Amit, V. Martin-Mayor, *Field Theory, The Renormalization Group and Critical Phenomena, 3rd ed* (World Scientific, Singapore, 2005).
[16] D. Gorbonos, R. Ianconescu, J. G. Puckett, R. Ni, N. T. Ouellette, N. S. Gov, Long-range acoustic interactions in insect swarms: an adaptive gravity model. New J. Phys. **18**, 073042 (2016).
[17] T. Vicsek, A. Czirók, E. Ben-Jacob, I. Cohen, O. Shochet, Novel type of

phase transition in a system of self-driven particles. Phys. Rev. Lett. **75**, 1226-1229 (1995).
[18]T. Vicsek, A. Zafeiris, Collective motion. Phys. Rep. **517**, 71-140 (2012).
[19]M. C. Marchetti , J. F. Joanny, S. Ramaswamy, T.B. Liverpool, J. Prost, M. Rao and R.A. Simha, Hydrodynamics of soft active matter. Rev. Mod. Phys. **85**, 1143-1189 (2013).
[20]H. Chaté, Dry aligning dilute active matter. Ann. Rev. Cond. Matter Phys. **11**, 189-212 (2020).
[21]G. Benettin, M. Casartelli, L. Galgani, A. Giorgilli, J. M. Strelcyn, Lyapunov Characteristic Exponents for smooth dynamical systems and for hamiltonian systems; a method for computing all of them. Part 2: Numerical application. Meccanica **15**, 21-30 (1980).
[22]E. Ott, *Chaos in dynamical systems* (Cambridge University Press, Cambridge UK 1993).
[23]M. Cencini, F. Cecconi, A. Vulpiani, *Chaos. From simple models to complex systems* (World Scientific, New Jersey 2010).
[24]J. B. Gao, Z. M. Zheng, Direct dynamical test for deterministic chaos and optimal embedding of a chaotic time series. Phys. Rev. E **49**, 3807-3814 (1994).
[25]J. B. Gao, J. Hu, W. W. Tung, Y. H. Cao, Distinguishing chaos from noise by scale-dependent Lyapunov exponent. Phys. Rev. E **74**, 066204 (2006).
[26]T. Bohr, Chaos and turbulence, in p. 157 of *Applications of Statistical and Field Theory Methods to Condensed Matter*, D. Baeriswyl, A. R. Bishop, J. Carmelo, eds. (Plenum, New York, 1990).
[27]M. C. Cross, P. C. Hohenberg, Pattern formation outside of equilibrium. Rev. Mod. Phys. **65**, 851-1112 (1993).
[28]H. G. Schuster, W. Just, *Deterministic chaos. An introduction. 4th ed* (Wiley-VCH, Weinheim, 2005).
[29]A. Cavagna, L. Di Carlo, I. Giardina, L. Grandinetti, T. S. Grigera, G. Pisegna, Renormalization group crossover in the critical dynamics of field theories with mode coupling terms. Phys. Rev. E **100**, 062130 (2019).
[30]A. Cavagna, L. Di Carlo, I. Giardina, T. S. Grigera, G. Pisegna, and M. Scandolo, Dynamical Renormalization Group for Mode-Coupling Field Theories with Solenoidal Constraint. J. Stat. Phys. **184**, 26 (2021).
[31]G. Baglietto, E. V. Albano, Finite-size scaling analysis and dynamic study of the critical behavior of a model for the collective displacement of self-driven individuals. Phys. Rev. E **78**, 021125 (2008).
[32]V. Holubec, D. Geiss, S. A. M. Loos, K. Kroy, F. Cichos, Finite-Size Scaling at the Edge of Disorder in a Time-Delay Vicsek Model. Phys. Rev. Lett. **127**, 258001 (2021).
[33]J. K. Hale, Theory of Functional Differential Equations (Springer, New York 1977).
[34]L. L. Bonilla, A. Liñán, Relaxation Oscillations, Pulses and Traveling Waves in the Diffusive Volterra Delay-Differential Equation. SIAM Journal on Applied Mathematics **44**, 369-391 (1984).
[35]A. Zomorodian, G. Carlsson, Computing persistent homology. Discrete Comput. Geom. **33**, 249-274 (2002).
[36]H. Edelsbrunner, J. Harer, *Computational Topology: An Introduction* (American Mathematical Society, 2010).
[37]M. Sinhuber, N. T. Ouellette, Phase Coexistence in Insect Swarms. Phys. Rev. Lett. **119**, 178003 (2017).
[38]J. Glimm, A. Jaffe, *Quantum Physics. A Functional Integral Point of View*, 2nd ed (Springer, 1987).
[39]J. M. Yeomans, *Statistical Mechanics of Phase Transitions* (Oxford Science Publications, Oxford UK, 1992).
[40]Y. A. Kuznetsov, *Elements of Applied Bifurcation Theory, 3rd ed*. (Springer, New York 2004).
[41]G. Dangelmayr, E. Knobloch, The Takens-Bogdanov bifurcation with $O(2)$-symmetry. Phil. Trans. R. Soc. Lond. A **322**, 243-279 (1987).
[42]T. Ihle, Kinetic theory of flocking: Derivation of hydrodynamic equations. Phys. Rev. E **83**, 030901(R) (2011).
[43]L. L. Bonilla, C. Trenado, Crossover between parabolic and hyperbolic scaling, oscillatory modes and resonances near flocking. Phys. Rev. E **98**, 062603 (2018).
[44]C. Trenado, L. L. Bonilla, A. Marquina, Bifurcation theory captures band formation in the Vicsek model of flock formation. arXiv:2203.14238.
[45]A.P. Solon, H. Chaté, J. Tailleur, From Phase to Microphase Separation in Flocking Models: The Essential Role of Nonequilibrium Fluctuations. Phys. Rev. Lett. **114**, 068101 (2015).
[46]R. Kürsten, T. Ihle, Dry Active Matter Exhibits a Self-Organized Cross Sea Phase. Phys. Rev. Lett. **125**, 188003 (2020).
[47]L. L. Bonilla, Two nonequilibrium phase transitions: Stochastic Hopf bifurcation and onset of relaxation oscillations in the diffusive sine-Gordon model, in p. 75 of *Far from equilibrium phase transitions*, L. Garrido, ed. (Lecture Notes in Physics 319, Springer, Berlin 1988).